

高性能光频域分布式光纤测试与传感技术研究进展

杨军^{1,3,4*}, 林蹉富², 邹晨², 喻张俊^{1,3,4}, 王云才^{1,3,4}, 秦玉文^{1,3,4}

¹广东工业大学先进光子技术研究院, 广东 广州 510006;

²哈尔滨工程大学物理与光电工程学院, 黑龙江 哈尔滨 150001;

³通感融合光子技术教育部重点实验室, 广东 广州 510006;

⁴广东省信息光子技术重点实验室, 广东 广州 510006

摘要 光频域反射(OFDR)是一种基于光调频连续波原理的分布式光纤测量技术,它利用扫频光干涉信号频率与光纤位置之间的傅里叶变换关系获取沿光纤分布的散射/反射/损耗、相位和偏振等特征信息,可进一步反演光纤感测的温度、应力/应变等外界物理场分布。相比于时域、相干域等分布式测量技术,OFDR的优点是可兼顾高空间分辨率、高测量灵敏度、长测量距离、大动态范围、高速响应等性能。回顾了OFDR的测量原理,综述了分布式测量噪声来源、空间点扩展函数退化机理以及测量误差与噪声抑制等OFDR性能提升关键技术;推导了基于OFDR分布式传感的测量极限,分析了提升传感精度与测量距离的若干方法;概述了国内外OFDR仪器发展现状及其在集成波导器件与保偏光纤等测试、光纤陀螺环内部应力传感等应用范例,最后展望了未来的若干研究方向。

关键词 光频域反射技术; 测量退化机理; 分布式传感极限; 光频域反射仪器; 高性能应用

中图分类号 O436

文献标志码 A

DOI: 10.3788/AOS231551

1 引言

分布式光纤测量是利用波导或介质中的散射、耦合等物理效应获取光纤和光学器件内部的损耗、偏振、色散等特征参量及其分布,或者感知外界物理、化学、生物等测量参量及其时空分布的一种高精度测试与传感技术。因其所具有的高灵敏、高分辨、大容量等优势,分布式光纤测试和传感技术自诞生以来就备受关注^[1-4]。时至今日,这项技术已经被广泛应用在桥梁和水坝等基础设施的结构健康监测^[5]、输电线路监测^[6]、油气开采与管道泄漏检测^[7-8]、海洋地球物理勘探^[9-10]以及各种光纤与光学器件性能表征与故障诊断^[11-13]等领域。

分布式光纤测量的核心技术难点是同时实现对待测参量的准确测量和空间位置的精确定位。分布式测量技术的特征之一体现在光学散射或耦合效应的测量原理上,散射效应分为背向瑞利散射(RBS)、前向/后向布里渊(Brillouin)散射、拉曼(Raman)散射三种,而耦合效应常指偏振串音(PC)、模间串扰分布等。它们既反映光路传输的状态与特性,可用于光纤与器件的

性能测试与缺陷评价;又常被用于各种参量的传感,如RBS、布里渊散射对温度和应变同时敏感,而拉曼散射则仅对温度具有特异性的敏感等^[4]。分布式测量技术的特征之二体现在空间位置定位技术上,除了最为基本和常用的时域(OTDR)、频域(OFDR)和相干域(OCDR)三种测量技术之外,研究人员还发展了混沌^[14]、编码^[15]等相关域定位技术^[16]以及时频调制复合域定位技术^[17]。

因此,近40多年中,先后涌现出30余种测量原理各异、技术性能互补、领域用途有别的分布式光纤测量技术,虽显纷繁复杂,但其技术内涵与分类主要由散射(或耦合)测量原理和空间定位技术二者来决定(表1)。

基本上,散射测量原理决定了分布式光纤测量的基本用途与应用场景;在此基础上,空间定位测量技术决定着测试与传感的核心性能参数。例如:OTDR测量技术采用单频光脉冲进行询问,根据测量脉冲飞行时间实现空间定位,因此测量距离与空间分辨率之间相互制约,存在本征矛盾,通常空间分辨率被限制在m量级^[47-48];OCDR测量将连续宽谱低相干光作为询问

收稿日期: 2023-09-14; 修回日期: 2023-10-25; 录用日期: 2023-11-08; 网络首发日期: 2023-11-17

基金项目: 国家重点研发计划(2022YFB3205200)、国家杰出青年科学基金(61925501)、国家自然科学基金(62127815)、广东省引进创新创业团队(2019ZT08X340)、广东省“珠江人才计划”(2019CX01X010)

通信作者: *yangj@gdut.edu.cn

表 1 分布式测试与传感技术的内涵与外延
Table 1 Connotation and extension of distributed testing and sensing technology

Location method		Time domain	Frequency domain	Coherent domain	Correlation domain (Chaos, coding)
	Intensity	(ν)OTDR ^[18]	OFDR ^[19]	OLCR/OCDR ^[20]	Chaos-OTDR ^[21]
		Φ -OTDR ^[22]	Φ -OFDR ^[23]		
RBS	Phase	TGD-OFDR ^[25] (coherent detection)		Φ -OLCR ^[24]	—
		CP-Phi-OTDR ^[26] (direct detection)			
	Polarization	POTDR ^[27]	POFDR ^[13]	PS-OLCR ^[28]	—
Raman scattering	Spontaneous	ROTDR ^[29]	ROFDR ^[30]	—	Chaos-ROTDR ^[31]
	Stimulated	ROTDA ^[32]	—	—	—
Brillouin scattering	Spontaneous	BOTDR ^[33]	BOFDR ^[34]	BOCDR ^[35]	Chaos-BOTDR ^[36]
	Stimulated	BOTDA ^[37]	BOFDA ^[38]	BOCDA ^[39]	Chaos-BOTDA ^[40] BOCDA(coding) ^[15]
Forward coupling/ scattering	Polarization crosstalk	POTDR ^[41]	OFDP ^[42]	OCDP ^[43]	—
	FSBS ^[44]	FSBS-OTDA ^[45]	—	—	—
	BGD	BGD-BOTDA ^[46]	—	—	—

Notes: FSBS indicates forward stimulated Brillouin scattering; TGD indicates time-gated digital; CP indicates chirped pulse; BOTDA indicates Brillouin optical time domain analysis; BOFDA indicates Brillouin optical frequency domain analysis; BGD indicates Brillouin dynamic grating; PS indicates phase-sensitive; OLCR indicates optical low coherence reflectometry; BOCDA indicates Brillouin optical coherence domain analysis; OCDP indicates optical coherence domain polarimetry; OFDP indicates optical frequency domain polarimetry.

光,本质上不存在测量距离与空间分辨率的矛盾,可提供 μm 级的空间分辨率,但在技术实现上受限于机械扫描装置,测量距离通常不超过 10 m ^[20];而 OFDR 测量则将频率连续调制(FMCW)的窄带激光作为问询光,它具有高光谱能量密度,极大提升了分布式测量的信噪比,理论上也同样实现了距离与空间分辨率的解耦。相比于 OTDR、OCDR 测量,OFDR 技术除具有 $10\ \mu\text{m}$ 级空间分辨率外,还可兼具 $-130\ \text{dB}$ 以上反射灵敏度、 $110\ \text{dB}$ 超大动态范围和 km 级测量距离等众多优势^[19,42,49]。

因此,自 1981 年 Eickhoff 等^[19]提出 OFDR 技术以来,作为最为重要的分布式测量技术之一,它已发展成为一种长距离、高精度、大动态、多参量的分布式光纤测试与传感技术^[50]。其发展进程由分布式测试^[13,51-56]与传感^[25-26,57-65]两条交织的路径组成,如图 1 所示,二者在测量原理与关键技术相辅相成,在测量对象与性能要求上又有所差异。

发展路径之一:分布式测试技术,围绕着光源扫频非线性校正与相位噪声抑制这一核心问题展开。里程碑事件包括美国 Luna 公司 Soller 等^[13]与韩国光州科学技术院 Ahn 等^[51]分别开创性地提出硬件、软件重采样方法来抑制扫频非线性;上海交通大学樊昕昱教授团队^[52]、北京理工大学董毅教授团队^[54]分别提出相位噪声补偿(PNC)、基于光锁相的扫频非线性抑制等经

典相位噪声抑制方法。经过后续不断的技术迭代,扫频非线性与相位噪声能够很好地被抑制;测试距离也逐渐提升至 $242\ \text{km}$ ^[55],最大测试容量(RRP,定义为测量距离和空间分辨率二者相除)可达 10^7 ^[56]。

发展路径之二:分布式传感技术。其进展可概括为多参量、高性能两种趋势,其一是基于 OFDR 拓展了扭转^[57]、磁场^[58]、折射率^[59]、双折射^[60]、应变^[61]与温度^[62-63]等多种参量的感知能力,已实现了数 10 种分布式物理、生化等参量的光纤传感器^[64];其二是上海交通大学何祖源教授团队^[25]提出时间门控法(TGD-OFDR)以及西班牙 Pastor-Graells 等^[26]提出啁啾脉冲技术(CP-Phi-OTDR)两项典型的高性能分布式声传感(DAS)技术,实现了最长 $108\ \text{km}$ 的传感距离, $3.6\ \text{p}\epsilon/\sqrt{\text{Hz}}$ 的超高振动灵敏度,RRP 最高可达 10^5 ^[65]。

本文力图沿着上述 OFDR 技术的发展脉络,在前期多篇综述文章的基础上,围绕高灵敏、高分辨、长距离、高频响等高性能 OFDR 技术的新进展,梳理其理论与技术框架,列举若干高性能、多参量 OFDR 分布式测试与传感的典型应用,并展望 OFDR 技术的潜在研究方向。

2 OFDR 测量原理

2.1 OFDR 测量技术

OFDR 测量技术来源于雷达领域中的 FMCW 技

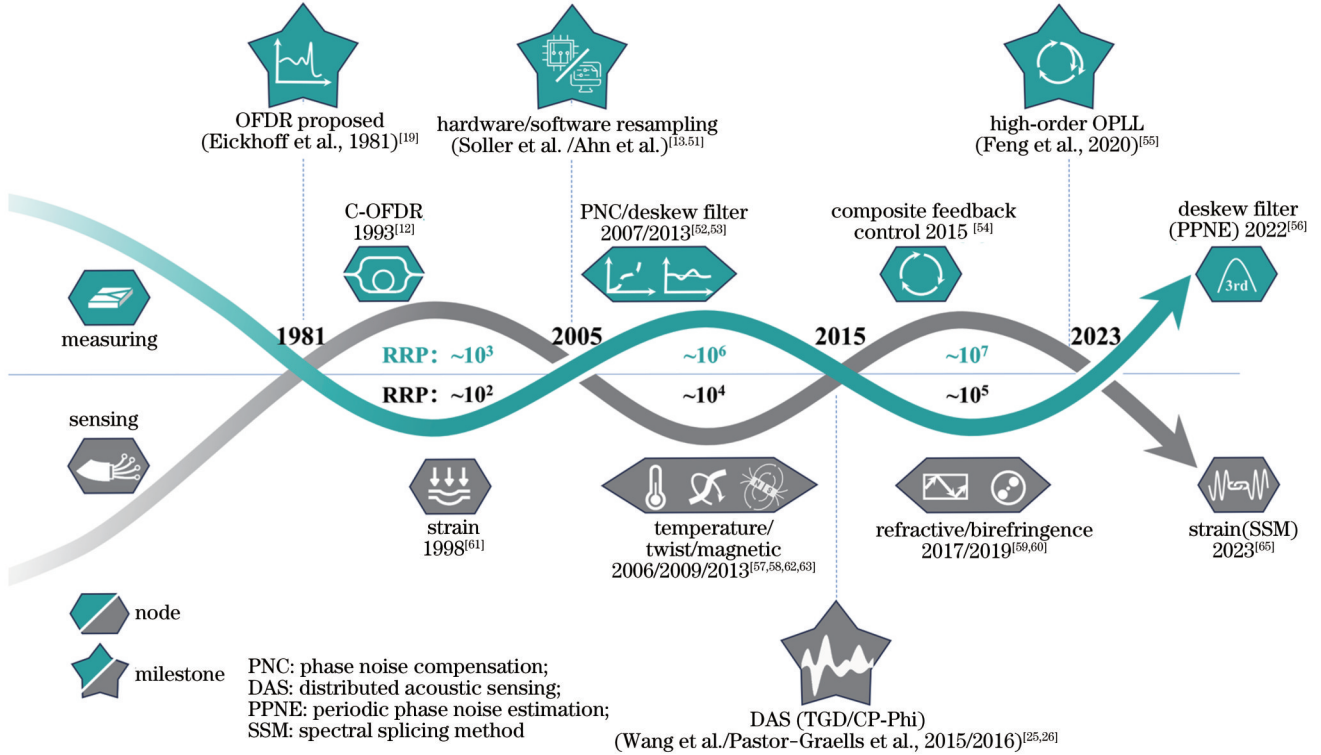


图 1 OFDR 技术发展进程与里程碑事件
Fig. 1 OFDR technology development process and milestones

术,其基本结构如图 2 所示。可调谐激光源(TLS)发出一束线性扫频光,扫频光通过耦合器被分为两路,一路进入参考臂作为本振(LO)光,另一路作为探测光注入待测光纤。本振光与 RBS、菲涅耳反射光等(图 2 中点 A)发生干涉,经探测器光电转换后形成拍频信号 $I_{\text{beat}}(t)$ 以及它的空间点扩展函数(PSF),即拍频信号的功率谱密度,表示^[66]为

$$\begin{cases} I_{\text{beat}}(t) = 2\sqrt{R} E_0^2 \cos(2\pi f_b t + C) \\ P(f, f_b) = 2RE_0^4 \delta(f - f_b) \end{cases}, \quad (1)$$

式中: E_0 是光电场强度; R 是反射率; $f_b = \gamma\tau$ 是时延为 τ 处的拍频信号的频率, γ 是光源的调谐速率; C 为常数; $\delta(f)$ 是单位冲激函数。此外,图 2 中 v 为光频率。

由式(1)可知,拍频信号 $I_{\text{beat}}(t)$ 的频率对应着光纤事件的发生位置(即延时 τ);拍频信号的幅度反映了该位置处的散射或反射强度。因此,对拍频信号 $I_{\text{beat}}(t)$ 进行频谱分析(或傅里叶变换),由 PSF 可得到光纤中的散射信息分布。

2.2 PFS 退化原因与分析

系统传递函数描述了输入信号如何被测量系统转换为输出信号。若将待测光纤视为输入的“物理”信号,那么 PSF 就是 OFDR 系统的传递函数(理想为单位冲激函数),表征 OFDR 系统测试光纤 RBS 时的核心性能指标。因此,PSF 的半高全宽定义了 OFDR 的空间分辨率,其频谱纯度表征了无杂散动态范围。理论上,OFDR 技术的最优空间分辨率 ΔL 和最大测量

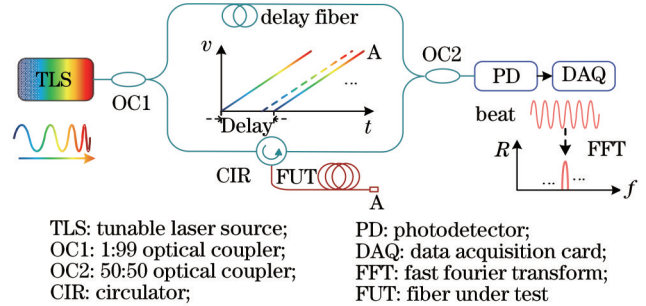


图 2 OFDR 的基本结构与原理示意图

Fig. 2 Basic structure and principle schematic of OFDR

长度 L_{max} 可以表示^[66]为

$$\begin{cases} \Delta L = \frac{c}{2n \cdot \Delta F} \\ L_{\text{max}} \propto \frac{c}{2n \cdot \Delta v} \end{cases} \text{ OR } \begin{cases} \Delta L = \frac{c \delta_f}{2n\gamma} \\ L_{\text{max}} = \frac{c f_s}{4n\gamma} \end{cases}, \quad (2)$$

式中: c 是真空中光速; n 是折射率; ΔF 是光源扫频范围; Δv 是激光器线宽; δ_f 是频谱分辨率; f_s 是采样率。

式(2)表明,空间分辨率既受限于光源调谐范围,又受限于信号探测的频率分辨率;而测量距离分别由光源线宽和信号采样频率共同决定。因此,理论上 OFDR 的测量性能由光源、光路、电路与信号探测等综合决定。

而实际测量时,OFDR 的性能还要受到各类噪声、畸变等非理想因素的影响^[67-68],具体表现为 PSF 的退化导致 OFDR 各项技术指标的大幅劣化。图 3 梳理了

OFDR 的噪声来源及其影响,其中,光源与外部环境中的噪声是导致 PSF 退化的主要因素。光源噪声主要包括相位噪声和强度噪声;相位噪声分为光源扫频非线性和本征相位噪声,二者均能导致空间分辨率的下降^[69]和

动态范围的退化,并限制测试距离^[70];强度噪声会破坏 PSF 的频谱纯度,进而限制系统的无杂散动态范围(SFDR)。外部环境噪声的作用效果等同于额外相位噪声的引入,同样会带来空间分辨率与动态范围的劣化。

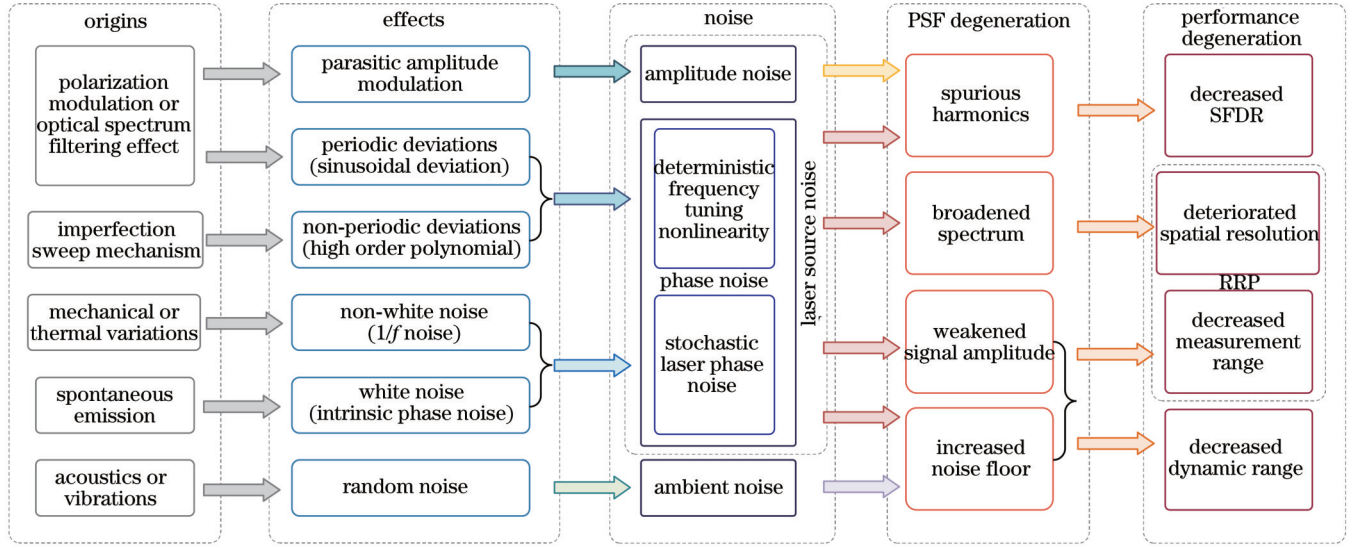


图 3 OFDR 系统中噪声的分类和影响

Fig. 3 Classification and influence of noise in OFDR system

因此,OFDR 的实际测量值将远远偏离式(2)所描述的理想值。噪声与畸变使测量性能之间产生了新的制约关系,如:光源非线性将决定空间分辨率;光源相位噪声决定了测量长度与空间分辨率(测试容量 RRP)之间存在的制约关系。

综上所述,高性能 OFDR 技术研究的关键是弄清 PSF 性能的退化机理,并充分抑制上述噪声与畸变对 PSF 的影响,使测量性能不断逼近理论极限。接下来,将对 OFDR 系统中的噪声来源及其 PSF 的退化机理进行详细讨论。

2.2.1 相位噪声

光源相位噪声是导致 PSF 退化的主要原因,PSF 退化带来了 OFDR 散射灵敏度、空间分辨率、测量长度等核心性能的劣化。光源的相位噪声分为两部分:

其一是扫频非线性,由不完美的光源扫频机制产生,又包含周期性和非周期性噪声,多以高阶多项式和不同频率正弦信号叠加的形式存在;其二是随机相位噪声,是原子自发辐射引起的相位随机抖动,表现为零均值、广义平稳的高斯过程。由此,光源的总相位噪声 $e_s(t)$ 可以写成

$$e_s(t) = \underbrace{\sum_{i=2}^{N_1} k_i t^i + \sum_{i=1}^{N_2} A_{pi} \sin(2\pi f_{pi} t)}_{\text{deterministic noise}} + \underbrace{r(t)}_{\text{random noise}}, \quad (3)$$

式中: t 是测量时间; k_i 是多项式的系数; A_{pi} 、 f_{pi} 分别是正弦项的幅度和频率; N_1 、 N_2 分别是相位噪声中包含的非周期性和周期性噪声的总量。

此外,光纤中的色散效应也会以附加扫频非线性的形式被引入到探测信号中,表示为

$$s_{\text{beat}}(t) = 2\sqrt{R} E_0^2 \cos \left[2\pi f_b t + \underbrace{e_s(t) - e_s(t - \tau)}_{\text{source-induced}} + \underbrace{2\pi^2 \gamma^2 v_g \beta_2 \tau t^2}_{\text{dispersion-induced}} \right], \quad (4)$$

式中: v_g 是群速度; β_2 是二阶色散系数。

为探究 PSF 的退化机理,一方面是扫频非线性的影响,以二阶多项式的非周期性噪声为例(色散噪声形式与其相同,不再单独列出),PSF 可以表示为

$$S(f, f_b) = P(f, f_b - m\tau t), \quad (5)$$

式中, m 为系数。此时,信号频率的啁啾变化使频谱展宽,位置识别精度下降,如图 4(a)、(b)所示。

另一方面,随机相位噪声对 PSF 的影响可以表示^[71]为

$$S(f, f_b) = G\delta(f) + \exp\left(-\frac{2\tau}{\tau_c}\right) P(f, f_b) + L(f) \left[1 - \exp\left(-\frac{2\tau}{\tau_c}\right) \right] \left\{ \cos[2\pi(f - f_b)\tau] + \frac{\sin[2\pi(f - f_b)\tau]}{\pi(f - f_b)\tau_c} \right\}, \quad (6)$$

式中： $G=(1+R)^2 E_0^4$ ； $L(f)=2RE_0^4 \tau_c / 1 + \pi^2 \tau_c^2 (f-f_b)^2$ ； τ_c 是相干时间； $\delta(f)$ 为冲激函数。

随着测量距离的增加,PSF的幅度呈指数型下降,并且相位噪声以拍频信号为中心呈洛伦兹型叠加在PSF上,系统性能指标迅速劣化,如图4(c)所示。

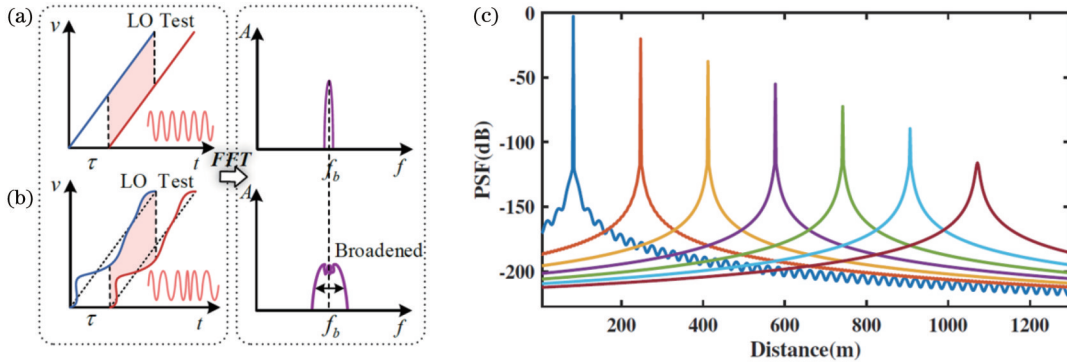


图4 光源相位噪声对PSF的影响^[66]。(a)(b)扫频非线性的影响；(c)随机相位噪声影响下的PSF(线宽为200 kHz、调谐率为5 THz/s)

Fig. 4 Influence of the laser source phase noise on the PSF^[66]. (a)(b) Influence of frequency tuning nonlinearity; (c) PSF under the influence of stochastic phase noise (linewidth is 200 kHz, tuning rate is 5 THz/s)

2.2.2 幅度(强度)噪声

幅度(强度)噪声包括相对强度噪声、寄生调幅^[72]等。相对强度噪声的影响通常低于相位噪声的影响；寄生调幅^[72]主要由光器件的光谱响应、光源的残余幅度调制导致,它是形成伪干涉峰、限制SFDR的主要因素。考虑寄生调幅时,拍频信号可表示为

$$s_{\text{beat}}(t) = 2\sqrt{R} E_0^2 A(t) A(t-\tau) \cos(2\pi f_b t + C), \quad (7)$$

式中： $A(t) = 1 + \sum_i B_i \cos(2\pi f_{mi} t)$ 是本振信号的幅度噪声,其中, B_i, f_{mi} 分别是幅度调制深度和调制频率; C 是常数。

当式(7)仅考虑一次谐波时,对应的PSF表示为

$$\begin{cases} S(f, f_b) = P(f, f_b) + 2RE_0^4 \Delta(f-f_b) \\ \Delta(f-f_b) = \\ B_i \delta(f-f_b \pm f_{mi}) + B_i^2 / 4 \delta(f-f_b \pm 2f_{mi}) \end{cases}, \quad (8)$$

式中： Δ 是寄生调幅引入的杂散信号。

由式(8)可知,寄生调幅改变了PSF的频谱纯度,严重影响了系统的SFDR,干扰待测光纤与器件特征信息的识别,极易造成光纤坏点、器件缺陷的误报。

2.2.3 环境噪声

OFDR系统测量时,外界环境中的声音或者振动扰动会随着光纤长度的增长而积累,并以相位噪声的形式存在于信号中,使PSF产生相位调制边带。环境噪声多为低频、多分量的扰动,因此表现为空间分辨率展宽与信号畸变。受环境噪声影响的PSF可以表示为

$$\begin{cases} S(f, f_b) = P(f, f_b) + 2RE_0^4 \Delta_\varphi(f-f_b) \\ \Delta_\varphi(f-f_b) = B_{\varphi i} \delta(f-f_b \pm f_{\varphi i}) + \\ B_{\varphi i}^2 / 4 \delta(f-f_b \pm 2f_{\varphi i}) \end{cases}, \quad (9)$$

式中, Δ_φ 是环境噪声引入的杂散信号; $B_{\varphi i}, f_{\varphi i}$ 分别是环境噪声引入的相位调制深度和调制频率。

上述的PSF退化因素引入了严重的待测参量空间、幅值畸变。光频域传感技术同样建立于光纤RBS信号提取的基础之上,因此高精度的噪声补偿是实现高性能分布式测试与传感的重要前提^[73]。

3 OFDR测试关键技术

针对相位噪声、幅度噪声、环境噪声导致的PSF退化问题,如今已有一系列的校正与补偿方法被提出。相位噪声分为扫频非线性与光源相位噪声,它是OFDR技术必须克服的重要难题,校正的核心思想是先监测、后校正^[51]。环境噪声的影响仅次于相位噪声,抑制环境噪声主要通过物理隔离、光学主动降噪两条思路实现。幅度噪声主要在超高精度测试中受到关注,可通过去趋势法进行抑制^[72]。接下来将围绕相位噪声及其抑制方法详细展开。

3.1 扫频非线性校正技术

OFDR测量时,高空间分辨率要求光源具有100 nm以上的宽调谐范围。上述光源一般采用外腔激光器结构,通过精细调节衍射光栅可以实现波长的无跳模扫描。因此,扫频机制固有的缺陷是造成激光频率偏离线性调谐的主要原因,它表现为扫频非线性,是OFDR测量中的主要噪声源。目前,已发展的扫频非线性的校正与补偿方法如表2所示。

扫频非线性最基本的解决方法之一是频率采样法^[13]。它将辅助干涉仪信号的过零点作为采集卡外部采样的时钟,以实现测量信号的均匀频率间隔采样。其优点是,采用硬件直接校正光源频率非线性,光源扫频和校正同步完成;但缺点是,光纤测量长度严重依赖辅助干涉仪臂长差(由奈奎斯特采样定理决定),测量

表 2 扫频非线性校正方法对比
Table 2 Comparison of frequency tuning nonlinearity compensation methods

Method	Year	Laser parameter		Performance	RRP	
		Linewidth	Tunable range			
Frequency sampling	Polarization diversity detection ^[13]	2005	200 kHz	37.5 nm	22 μm@35m	1.59×10 ⁶
	HTCM ^[51]	2005	100 kHz	1 nm	3 cm@3 m	1.00×10 ²
	Envelope detection ^[74]	2009	1 MHz	1 nm	0.4 cm@150 m	3.75×10 ⁴
Resampling algorithm	NUFFT ^[75]	2012	1.2 MHz	2 nm	5 cm@50 m	1.00×10 ⁹
	Time-scale factor ^[76]	2019	100 kHz	9 nm	0.17 mm@155 m	9.12×10 ⁵
	Intergrated point ^[77]	2020	—	20 nm	41 μm@50 m	1.22×10 ⁶
	Equal frequency ^[78]	2021	200 kHz	130 nm	21.3 μm@191 m	8.97×10 ⁶
	Interpolation frequency ^[79]	2023	200 kHz	150 nm	14.9 μm@100 m	6.71×10 ⁶

Notes: HTCM indicates Hilbert transformation compensation method, and NUFFT indicates non-uniform fast Fourier transform.

距离难以超过 100 m。

为了克服频率采样法的限制, Ahn 等^[51]提出了软件重采样方法, 由此发展出一系列衍生技术^[74-76]。该方法对辅助干涉仪和测量干涉仪的信号进行同时采集, 从前者提取扫频光源的时变频率信息, 利用此光频信息对测量信号进行插值完成重采样。光频提取方法主要有希尔伯特变换^[51]、包络法^[74]、时间-尺度因子法^[76]等, 它们的共性问题在于, 光频信息提取准确度的提升必然伴随着算法复杂度的增大。插值算法中三次样条插值最为常见^[76], 但其缺陷在于需要

较长的运算时间来保证高插值精度。为此, 具有高速处理优势的非均匀傅里叶变换(NUFFT)^[75]也被引入, 这样能提高插值权重计算效率, 减轻运算负担, 然而这依然属于数据插值算法, 同样需要平衡处理时间与插值精度。较为典型的结果包括: 英国学者利用等光频重采样在 191 m 距离处实现了 21.3 μm 的高空间分辨率^[78]。此外, 广东工业大学杨军教授团队^[79]也提出了优化的插值重采样方法, 在 100 m 光纤全长获得了最优 14.9 μm 的高空间分辨率, 如图 5 所示。

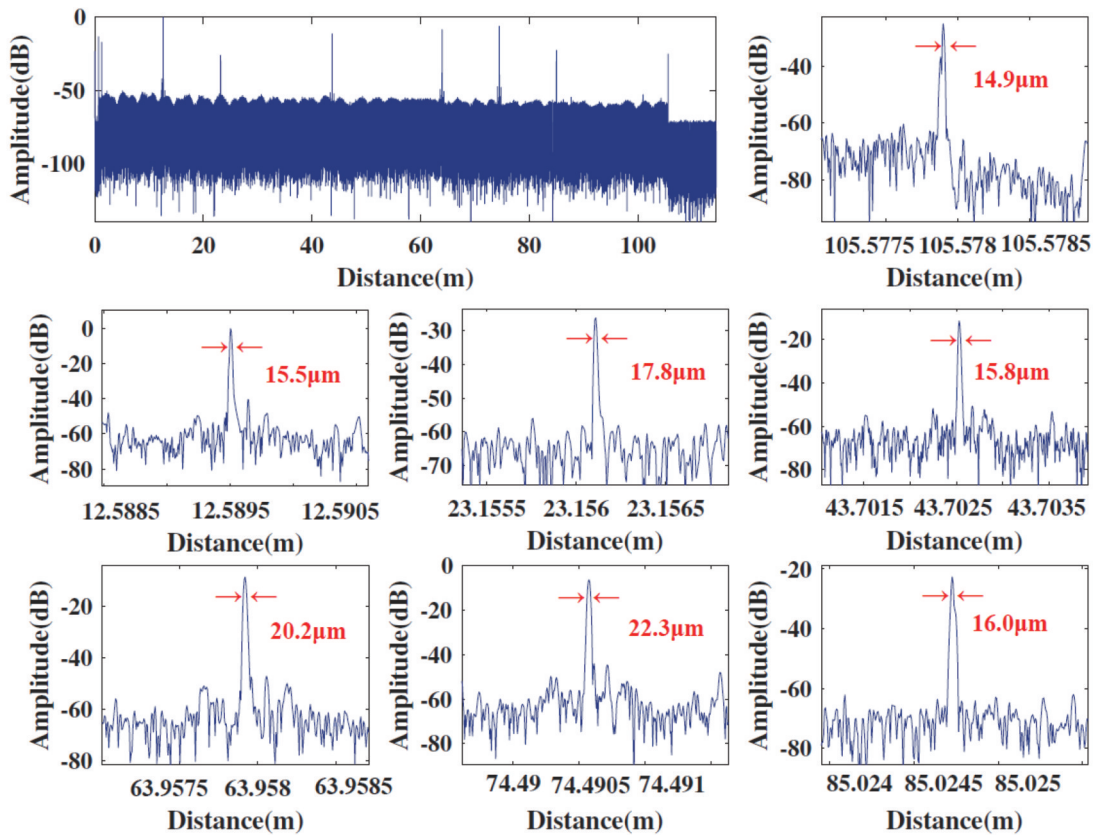


图 5 测量距离为 100 m 时各位置处的补偿结果^[79]
Fig. 5 Compensation results at each position when the measurement distance is 100 m^[79]

尽管软件重采样算法能够有效去除扫频非线性,但其校正误差会随着测量长度的增加而逐渐积累,由于无法消除光源的相位噪声,当测量百 m 级以上光纤时,空间分辨率将迅速劣化,甚至导致测量失效;此外,高精度重采样算法的计算复杂度高、运算量大、耗时长,不适合实时测量。

3.2 相位噪声抑制技术

在 OFDR 系统中,PSF 受光源相位噪声影响随着

测量距离不断接近光源相干长度的程度而增大。宽调谐光源虽然能够实现高空间分辨率的测量,但其线宽(对应光源相干长度)限制了系统的测量距离。因此,长距离测量时,OFDR 对光源相干性要求更加严苛,光源相位噪声将成为系统性能的主要限制因素。为了摆脱光源相位噪声的影响,扩展 OFDR 的测量距离,国内外研究人员进行了许多研究,研究出的相位噪声校正方法的具体细节如表 3 所示。

表 3 相位噪声校正方法对比
Table 3 Comparison of phase noise compensation methods

Method	Year	Laser parameter		Performance	RRP	
		Linewidth	Tunable range			
External modulation	SSB-SC ^[80]	2008	2 kHz	16 GHz	cm-level@5 km	5.00×10^5
	OPLL ^[49]	2019	5 kHz	1 GHz	72 cm@200 km	2.78×10^5
Active servo-loop	High-order OPLL ^[55]	2020	5 kHz	8 GHz	4.3 cm@242 km	5.63×10^6
	Multi-loop ^[81]	2021	A few kHz	60 GHz	1.67 mm@3.23 km	1.93×10^6
	Dual-loop ^[82]	2021	5 kHz	8.2 GHz	3.7 cm@185 km	5.00×10^6
PNC-based method	Bandwidth-division ^[83]	2011	4 kHz	15 GHz	5 cm@40 km	8.00×10^5
	Hardware-adaptive ^[84]	2019	1 kHz	2 GHz	7 cm@100 km	1.43×10^6
Deskew-filter-based algorithm	Deskew filter ^[53]	2013	1 kHz	1 GHz	1.6 m@80 km	5.00×10^4
	Optimized deskew filter ^[85]	2014	1 kHz	1 GHz	0.8 m@80 km	1.00×10^5
	PPNE deskew filter ^[56]	2022	60 kHz	375 GHz	522 μm @8 km	1.53×10^7

Notes: SSB-SC indicates single sideband with a suppressed carrier, and OPLL indicates optoelectronic phase-locked loop.

从信号探测与接收的角度出发,可以利用后处理算法实现相位噪声的补偿。如:上海交通大学樊昕昱教授团队^[83]提出相位噪声补偿光频域反射仪(PNC-OFDR)算法并将其移植到现场可编程门阵列(FPGA)上,实现了实时解调,在 100 km 的测试范围(系统能够测量的最大长度)内达到了 7 cm 的空间分辨率^[84]。该方法的不足之处在于,当偏离最佳补偿点时,空间分辨率会由于残余相位噪声而产生退化。此外,天津大学的丁振扬团队^[85,53]将去斜滤波器算法引入 OFDR 中,在 80 km 处实现了 0.8 m 的空间分辨率,但随着距离增加,空间分辨率与理论值相比劣化严重。上述方法的共性问题,是由于光源相位噪声的估计精度不足,因此空间分辨率难以进一步提升,进而导致测量容量均无法突破 10^7 。

为了更准确地实现光源相位噪声的估计,广东工业大学杨军教授团队^[56]提出基于高精度周期性相位噪声估计的去斜滤波器(PPNE-deskew-filter)方法。光源相位噪声能够通过高阶泰勒展开而精确进行估计,其信息随着展开阶数的提高而丰富;但是高阶展开中的微分运算对随机噪声的放大作用会使相位噪声中周期性噪声等有效特征信息被覆盖,反而会影响相位噪声估计精度。为此,首先利用参考信号非线性相位的多项式拟合结果构建误差函数,确定最优平滑窗长;其次通过具有最优平滑窗长的移动平均滤波器滤波,抑

制高阶微分过程中的随机噪声放大效应,保留相位噪声中有效的细节信息;最后依靠三阶泰勒展开方法提高光源相位噪声尤其是周期性相位噪声的估计精度。准确地获取光源相位噪声信息后,利用频率响应为 $Q_y(f) = \exp(j\pi f^2/\gamma)$ 的去斜滤波器对相位噪声进行去除。算法的流程图如图 6 所示。

基于该方法构建的 OFDR 系统的测量结果如图 7 所示,光源采用外腔式可调谐激光器(Santec, TSL-770, 线宽为 60 kHz, 扫频范围为 3 nm)。该系统在 8 km 的待测光纤全长范围内均保持亚 mm 级空间分辨率(光纤末端的空间分辨率也可达 522 μm),测量容量首次超过 10^7 。

4 基于 OFDR 的分布式传感技术

信号光在光纤中传输时,任何加载在光纤上的外界物理场(如温度、应变、振动、磁场等)均会导致光束传输特性发生变化。作为一种高精度、分布式的光纤 RBS 测试技术,OFDR 不仅能够测量待测光纤中光路损耗、偏振、相位等传输特性的时空分布,还可以反演获得外界待测量,实现物理场的分布式感知。接下来将简要地介绍 OFDR 分布式温度、应变参量传感方法与技术体系;着重论述 OFDR 传感性能的理论极限及提升方法。

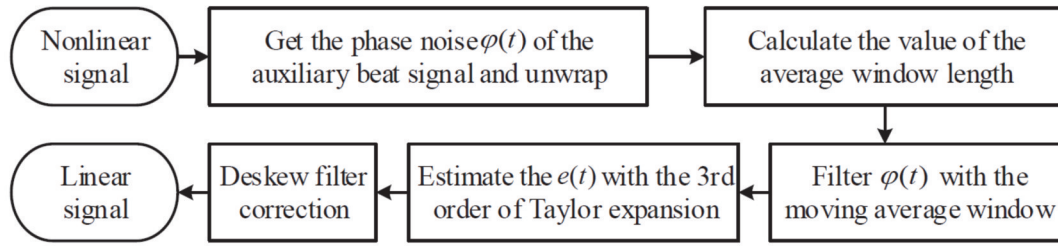


图 6 PPNE-deskew-filter算法流程图^[56]

Fig. 6 Flowchart of PPNE-deskew-filter algorithm^[56]

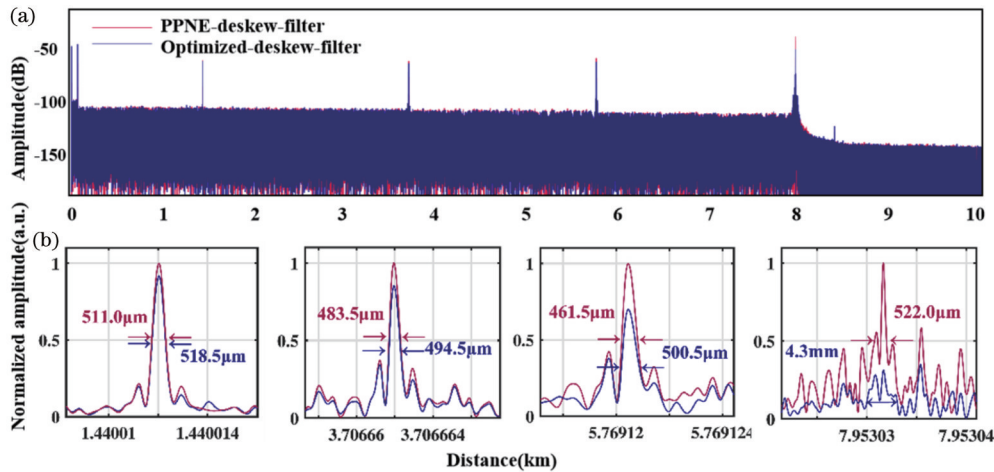


图 7 测量距离为 8 km 时的补偿结果^[56]。(a)基于 PPNE 的去斜滤波器与优化去斜滤波器结果对比；(b)空间分辨率对比

Fig. 7 Compensation results of 8 km measurement distance^[56]. (a) Comparison of the results by optimized deskew filter and PPNE deskew filter; (b) comparison of spatial resolution

4.1 基于 RBS 的温度与应变传感原理

当外界待测温度、应变作用于敏感光纤时,借助光纤热膨胀、弹性形变、热光效应以及弹光效应可将待测物理场的变化映射至 RBS 光学参量的变化。其中:光纤热膨胀、弹性形变将分别导致光纤物理长度或传输光程的变化;热光或弹光效应将使光纤折射率发生改变;较大应力/应变将使 RBS 强度发生变化。因此,不论光纤长度还是折射率的变化,都将传递至 RBS 的传输光程或相位上,最终表现为 OFDR 测得的 RBS 的光程(或相位)、强度(幅值)和光谱分布三个信息维度的变化,如图 8 所示。

上述的三个信息维度是 RBS 在空域、谱域、相位域的映射,是 RBS 信息的三种表现形式。如图 9 所示(其中, f_{R-sta} 和 f_{R-end} 分别为起始频率和终止频率),随着应变或温度的加载, RBS 分别表现为强度变化、光谱频移 Δf 、差分相位变化 $\Delta\varphi$ 。空域的 RBS 强度变化是非线性的,无法定量反演应变或温度变化。除此之外,检测光谱频移、差分相位变化均可以定量地获取分布式应变或温度信息。外界应变变化 $\Delta\varepsilon$ 或温度变化 ΔT 带来的 RBS 的光谱频移 Δf 与差分相位变化 $\Delta\varphi$ 分别表示^[86-88]为

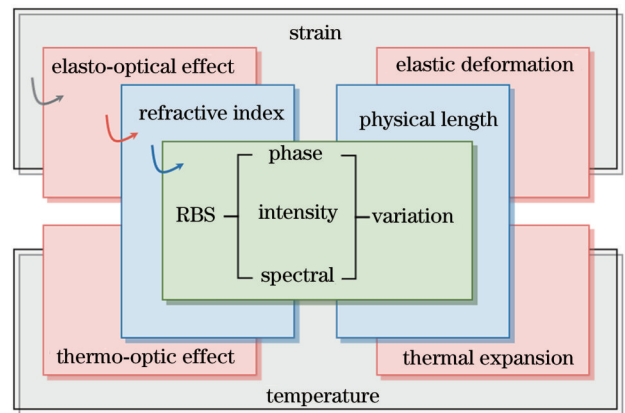


图 8 基于 RBS 传感的待测参量传递过程

Fig. 8 Transfer process of parameter under test based on RBS sensing

$$\begin{cases} \Delta\varepsilon = \frac{K_\varepsilon}{D} \cdot \Delta\varphi = -\frac{1}{0.78f_c} \cdot \Delta f \\ \Delta T = \frac{K_T}{D} \cdot \Delta\varphi = -\frac{1}{6.92 \times 10^{-6} f_c} \cdot \Delta f \end{cases}, \quad (10)$$

式中: D 是相位距离差分的间隔; K_ε 是应变灵敏度系数; K_T 是温度灵敏度系数; f_c 是询问光中心频率。当询问光中心波长为 1550.12 nm, 光纤折射率为 1.46 时,

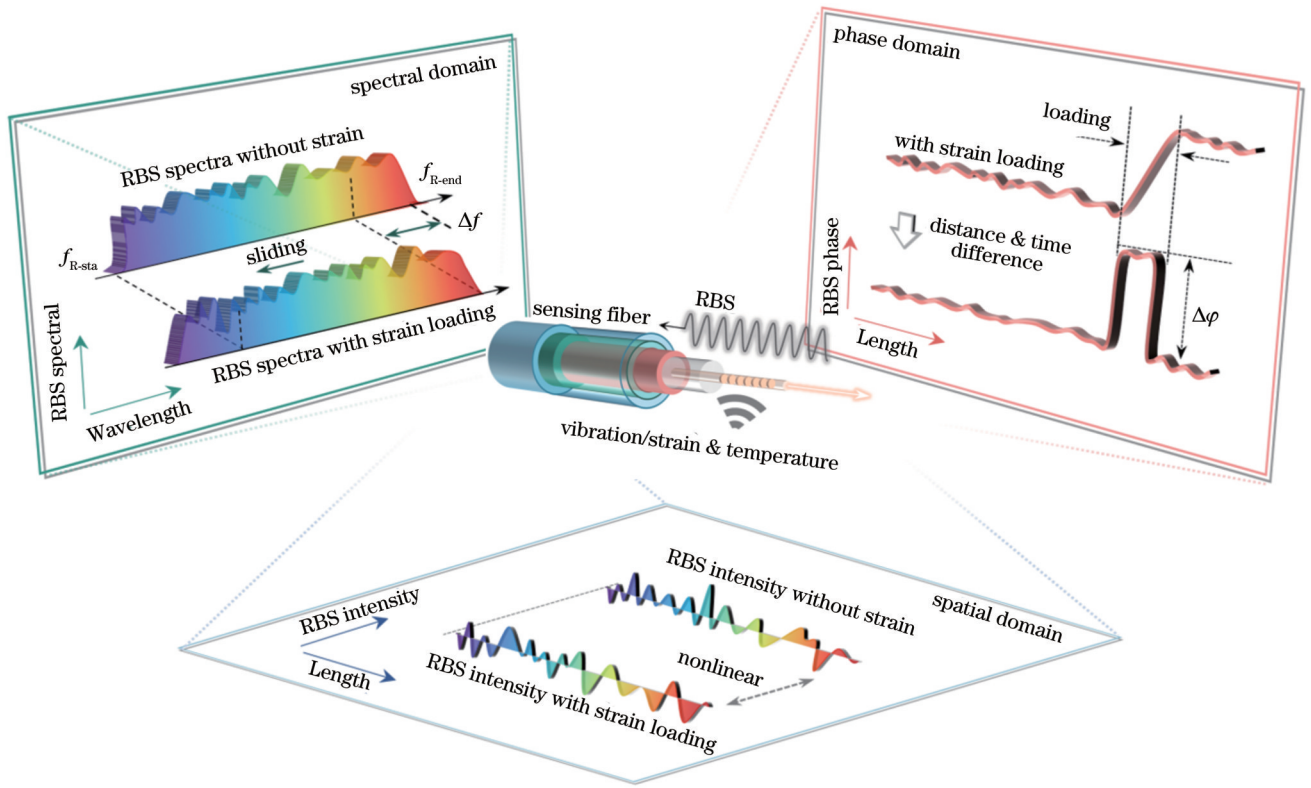


图9 RBS的空域、谱域、相位域映射关系示意图

Fig. 9 Mapping diagram of RBS in spatial domain, spectral domain and phase domain

$K_\epsilon = 110.37 \text{ ne} \cdot \text{m}/\text{rad}$, $K_T = 0.0124 \text{ }^\circ\text{C} \cdot \text{m}/\text{rad}$.

待测量与光纤 RBS 的作用过程揭示了 OFDR 传感技术的两个局限性:第一,OFDR 只能实现相对变化量的传感,必须在时间或空间分布上具有参考的 RBS 信息,如 RBS 相位的距离差分或相邻时刻差分。第二,OFDR 是一种非特异性的传感技术,众多的外界因素都会作用于 RBS 并使其发生变化。这会导致基于 OFDR 的单参量解调性能稳定性差、易受干扰,不具备多参量解耦的能力。解决这一问题的方法是增加 RBS 信息维度或引入特异性维度,如,通过对 RBS 的偏振检测实现扭转量的剥离以及引入保偏光纤解耦温度与应变^[89]等。

4.2 OFDR 传感性能分析

传感长度、空间分辨率、幅值精度、幅值范围、频率响应是 OFDR 传感性能的 5 个核心技术指标,它们之间的关系如图 10 所示。

4.2.1 内在本征因素的制约

限制 OFDR 传感核心技术指标的因素主要分为内在本征因素与外部测量影响两大类。内在本征因素指传感与解调机理、本征噪声源等,它只能被抑制而无法被消除;外部测量影响指硬件性能瓶颈、环境干扰等非理想因素,随着硬件更新与技术进步有望被彻底消除。

已报道的本征因素包括:传感长度与频率响应、传感带宽与传感精度、空间分辨率与精度以及幅值范围

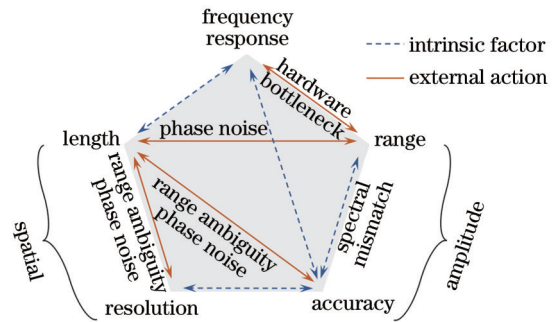


图 10 OFDR 传感技术核心性能指标关系示意图

Fig. 10 Relationship diagram of OFDR sensing method performance

与精度 4 个方面的相互制约关系。事实上,OFDR 传感性能(传感长度、空间分辨率、精度、范围、速度等)的核心指标之间均存在制约关系。一般 OFDR 系统中的散粒噪声决定了其理论性能的上限。

因此,为了量化表征 OFDR 传感的性能极限与制约权衡关系,以应变传感为例,广东工业大学杨军教授团队^[90]提出将散粒噪声作为最小噪声源,通过克拉美罗下界获取期望的方差下界,进而获得上述核心技术性能之间的定量表达式,表示为

$$\xi \geq \sqrt{\frac{c^3}{n^3 f_c^2} \cdot \frac{1}{R_{SN}} \cdot \frac{1}{\Delta L_\epsilon^3} \cdot \frac{1}{\Delta F}}, \quad (11)$$

式中: ξ 为应变传感精度; ΔL_ϵ 为应变空间分辨率; R_{SN}

为 RBS 测量信噪比。

式(11)描述了应变精度与其他性能之间的关系。其中:频率响应 H 、传感长度 L 包含于 RBS 信噪比 (SNR, R_{SN}) 中,考虑光纤衰减与噪声带宽,有 $R_{SN} \propto (L \cdot H)^{-1}$;幅值范围 W_ϵ 与 ΔF 成正比。通过式(10)进行换算,式(11)可以改写为定性表达式:

$$\xi \propto \sqrt{\frac{4\pi c^3}{0.78n^3 f_c^2} \cdot \frac{L}{\Delta L_\epsilon^3} \cdot \frac{1}{W_\epsilon} \cdot H} \quad (12)$$

在本征噪声的限制下,应变精度的平方在数值上与传感长度、带宽成正比,与应变测量范围和空间分辨率的立方成反比。在充分抑制测量非理想制约因素的

前提下,对式(11)进行了实验验证。实验分别通过调节光功率控制信噪比、调节扫频范围、修改窗口长度控制应变空间分辨率,逐一验证系统参数对应变精度的影响,所得结果如图 11 所示(图中用 SR 表示应变空间分辨率)。

需要特别说明的是,图 11(a)中,当光功率过低时,电路噪声代替散粒噪声成为主导噪声,故不再符合式(11)给出的理论规律。除此之外,实验结果很好地证明了公式的正确性。式(11)是基于 RBS 的特性与 OFDR 应变解调原理推导得到的,其中的参数定性制约关系可推广至 Φ -OFDR、CP- Φ -OTDR、TGD-OFDR 等各种基于 RBS 的传感技术中^[91]。

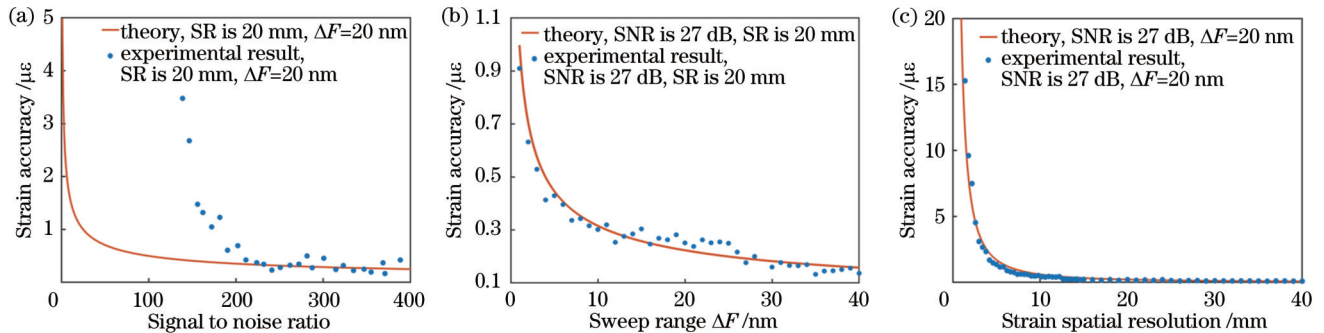


图 11 应变精度测量极限关系验证。(a)信噪比与应变精度的关系;(b)扫频范围与应变精度的关系;(c)应变空间分辨率与应变精度的关系

Fig. 11 Validation of extremal relationships for strain accuracy measurements. (a) Signal-to-noise ratio versus strain accuracy; (b) sweep range versus strain accuracy; (c) strain spatial resolution versus strain accuracy

4.2.2 外部非理想因素的制约

限制 OFDR 系统传感性能的主要非理想因素是距离模糊与 RBS 幅度畸变。距离模糊是由扫描速度波动、被测量加载等因素造成的 RBS 光程上的偏差(即模糊),过量的距离模糊会导致光纤取样空间上的参考与测量解调窗口在光纤长度上完全错位,从而丢

失 RBS 光谱的相关性^[92]。RBS 畸变指的是残余相位噪声、伴生幅度调制、偏振衰落导致的 RBS 光谱相关性退化现象。上述非理想因素同样带来了 OFDR 传感性能(传感长度、空间分辨率、精度、范围、速度)的退化。非理想因素的影响、类别、作用机理、噪声源如表 4 所示。

表 4 OFDR 传感性能制约因素分析

Table 4 Analysis of constraints on OFDR sensing performance

Performance degradation	Mechanism	Noise	Effect	Origins
Poor sensing distance and spatial resolution	Range ambiguity, RBS distortion	Phase noise	Nonlinear frequency sweeping	Tunable laser Environmental Strain/Vibration Temperature ...
			Phase noise of laser	
			Thermo-optic effect	
			Elasto-optical effect	
			Dispersion	
Strain accuracy and range degradation		Amplitude noise	Parasitic amplitude modulation	...
			Polarization fading	
			Spectral filtering of device	
			...	

4.3 OFDR 性能提升方法

接下来,从光纤 RBS 的三个信息维度出发,分别简要介绍强度、光谱、相位三种解调方法并阐述其优劣势;以 OFDR 传感性能(传感长度、空间分辨率、精度、

范围、速度)为切入点,列举典型的外部非理想因素抑制与优化方法。

4.3.1 解调原理概述

强度解调法是早期 DVS (distributed vibration

sensing)系统的解调方法^[93]。由于光纤 RBS 强度变化与待测量不具有线性关系,强度解调法无法定量获知待测量的数值,只能定位待测量加载的位置^[94]或感知振动频率^[95-96]。具体方法为:利用振动信号调制强度谱所产生的旁瓣,通过空域互相关得到振动频率。强度解调法具有流程简单、易实现的优点;但实际应用过程中,该方法的抗干扰能力弱,受相位噪声、强度噪声、偏振衰落等各种因素影响时很容易出现 RBS 强度谱的退相关,导致解调精度退化或出现无法解调的故障。

光谱解调法由 Froggatt 等^[61]在 1998 年提出,如图 12 所示,其中:DAQ 表示数据采集卡;RAM 表示随机存取存储器;Amp 表示幅值。光谱解调法通过设定空域窗口来提取特定位置处的 RBS 信息,从而实现空间解耦,再将其变换至谱域进行互相关获得光谱偏移量,进而实现分布式应变信息的解调。光谱解调法中,应变空间分辨率与散射空间分辨率的比值通常设

定为 10~50,以保证较高的互相关信噪比。得益于百 nm 级宽谱的 FMCW 询问光,其应变空间分辨率仍能达到 0.5 mm^[97],可轻松实现 $\pm 10000 \mu\epsilon$ 的大范围静态应变解调^[98]。应变精度与空间分辨率呈反比例关系,典型值为: $\pm 8.7 \mu\epsilon @ 1 \text{ mm}^{[97]}$ 、 $\pm 1.0 \mu\epsilon @ 1 \text{ cm}^{[65]}$ 。光谱解调法也可以实现振动的测量,但这是以应变精度、应变测量范围为代价的;典型的参数是:应变测量范围 $-1000 \sim 1000 \mu\epsilon @ 20 \text{ Hz}$ 、 $-200 \sim 200 \mu\epsilon @ 100 \text{ Hz}^{[92]}$ 。

光谱解调法兼具高精度、大范围与高速度,其解调性能可根据实际需求调整,并通过搭配不同的询问方式与参数进行平衡或侧重,其本质上是激光器在窄线宽、大范围、快扫描速度之间的权衡。该方法的主要局限在于:1)受限于相位噪等因素,导致传感距离难以扩展^[65,73];2)受限于距离模糊、光谱失配、相关性退化等因素,导致应变量与精度无法进一步提升^[91,97-102]。

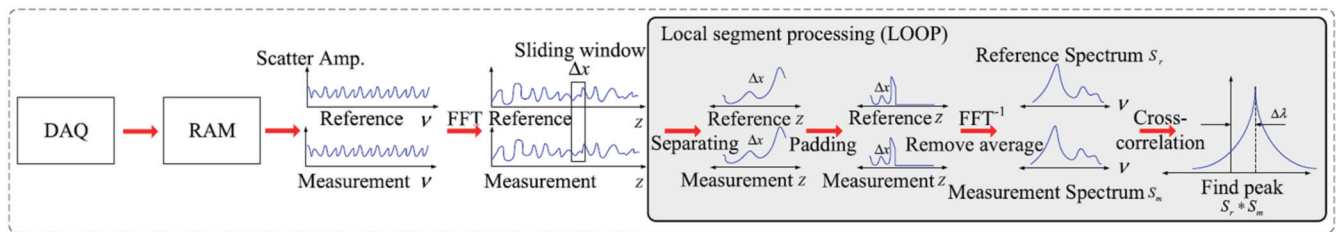


图 12 RBS 光谱解调流程^[103]

Fig. 12 Demodulation process based on RBS spectral^[103]

相位解调法最早是 Taylor 等^[104]基于 Φ -OTDR 技术提出的,而应用于 OFDR 技术是在 2015 年 Wang 等^[25]提出 TGD-OFDR 技术后,该方法侧重于长距离、高精度的振动传感^[105]。2017 年, Li 等^[23]也提出了基于 FMCW 的 Φ -OFDR 技术,其亮点是具有超高的空间分辨率与精度。基于 FMCW 的相位解调法近三年得到了快速发展,包括但不限于:人工神经网络^[106]、差分相对相位法^[107]、ARC-DSM (arctangent function and differential-self-multiplying) 算法^[108],其核心思想都是先获取沿光纤长度变化的散射相位,再通过距离或时间差分获取分布式应变信息,典型的解调流程如图 13 所示。相较于光谱解调法,相位解调法以散射空间分辨率为最小解调单元,在相同扫频范围下取得的应变空间分辨率要优于光谱解调法^[109]。它能够实现的传感长度在 50 m 以内,空间分辨率最小可达 $223 \mu\text{m}^{[110]}$,应变精度的典型值为 $\pm 5 \mu\epsilon @ 1 \text{ mm}^{[111]}$ 。受限于相位解调区间,该方法单次测量能够实现的应变变量程仅为 $25 \mu\epsilon^{[107]}$,然而通过对应变加载过程的连续观测累积,最大可以实现 $14000 \mu\epsilon$ 的解调^[112]。相位解调法具有超高的空间分辨率与精度,但同样受限于可调谐激光器的巨大扫频非线性与相位噪声,很难实现长距离的测量,且其单次应变变量程较小,只能牺牲测试频率响应以实现应变变量程扩展,二者呈现出制

约关系。

依据强度、光谱、相位三种解调方法,可以对现有 OFDR 传感技术归类分析,所梳理的技术脉络如图 14 所示。

OFDR 传感技术的典型性能数据如表 5 所示。在三种主要方法中:强度解调法局限于其传感原理,定量困难且精度较低,是 RBS 信息最初的认知与利用方式。相位解调法表现出极高的精度和亚 mm 级空间分辨率的优势,并具有动态传感能力;但其缺陷是测量距离(数十 m)与单次应变测量范围严重不足。光谱解调法技术体系成熟,机理清楚,性能均衡;优势在于极大的单次应变测量范围与高空间分辨率,同时也能保有不俗的精度和测试距离,具有长时准静态应变观测能力;劣势在于动态传感能力弱,但已有部分方法克服了这一缺陷。本文着重论述光谱解调法中各技术的发展情况,少量涵盖相位、强度解调法。

4.3.2 OFDR 传感距离扩展技术

基于 OFDR 的分布式传感技术继承了 OFDR 测量高精度、高动态范围的优势,也同时受限于 OFDR 中的扫频非线性、相位噪声等因素。目前 km 级以上的传感距离仅在 TGD-OFDR 等外调制方案中出现^[113],OFDR 的传感距离长期保持在数百 m 而难以进一步提升^[50],其根本原因在于:1)校正算法残余的非线

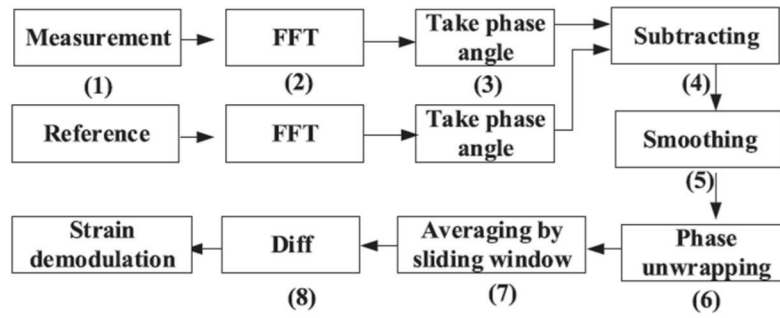


图 13 基于 RBS 相位的差分相对相位法解调流程^[107]

Fig. 13 Differential relative phase demodulation process based on RBS phase^[107]

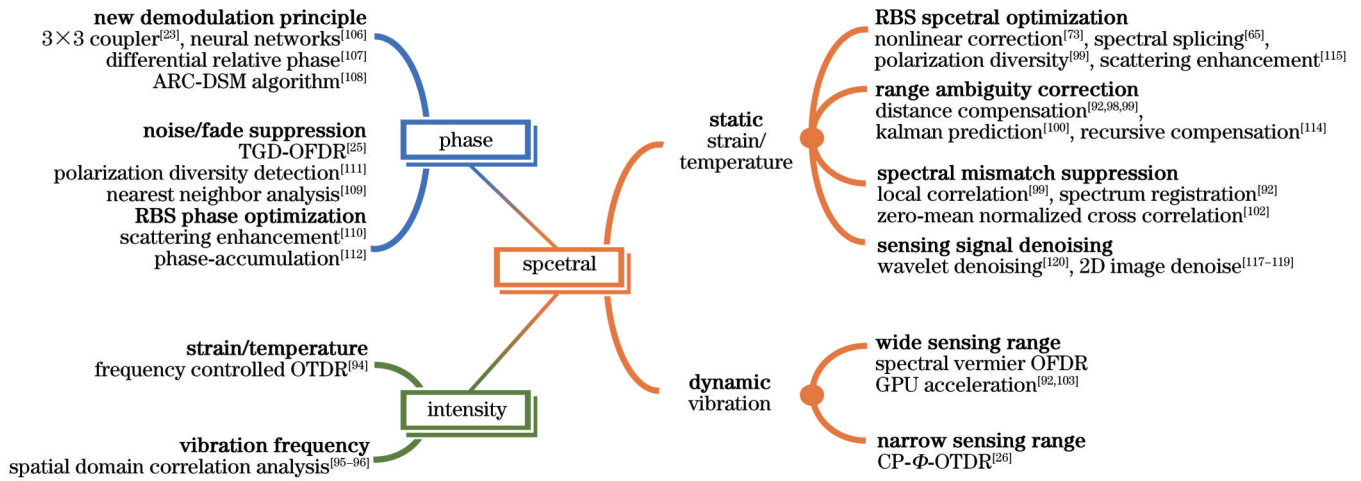


图 14 OFDR 传感技术脉络

Fig. 14 OFDR sensing technology development thread

表 5 OFDR 传感性能一览

Table 5 Overview of OFDR sensing performance

	Method	Year	Length	Spatial resolution	Strain/Temperature		Rate
					Range	Accuracy	
Intensity	Spatial domain correlation analysis ^[96]	2016	42 km	11.6 m	N/A	N/A	500 Hz
	Frequency controlled OTDR ^[94]	2009	8 km	N/A	2 με 0.22 °C	89 ne 0.01 °C	Static(~s)
Phase	Phase accumulation ^[112]	2022	13.5 m	18 mm	14000 με	0.48 με	Static(~s)
	Scattering enhancement ^[110]	2022	10.4 m	0.2 mm	1400 με	1.3 με	Static(~s)
	Polarization diversity detection ^[111]	2023	2.5 m	1 mm	400 με	5 με	Static(~s)
Spectral	Spectral splicing ^[65]	2023	1 km	1 cm	10000 με	±1.1 με	Static(~s)
	Nonlinear correction ^[73]	2014	300 m	7 cm	568 με 50 °C	2.3 με 0.7 °C	Static(~s)
	Kalman prediction ^[100]	2022	50 m	5 mm	10000 με 450 °C	5 με 0.5 °C	Static(~s)
	Zero-mean normalized cross correlation ^[102]	2018	22 m	1.6 cm	5000 με	50 με	Static(~s)
Spectral	Distance compensation ^[98]	2022	10.4 m	2 mm	10000 με	N/A	Static(~s)
	Spectral vernier	2023	10 m	20 cm	10856 με	0.4 με 19 ne/√Hz	2.4 kHz
	Spectrum registration & GPU (graphics processing unit) ^[92]	2019	1.2 m	5 mm	200 με 1000 με	20 με	100 Hz 20 Hz

性相位噪声带来了严重的 RBS 畸变,在长距离 OFDR 传感中尤为突出,是限制传感距离的主要原因;2)距离模糊量沿光纤长度累积,长距离传感必须具备更高精度的距离模糊校正方法。尽管已有大量的距离模糊校正方法被提出^[91,97-99,113],但没有本质上提升 OFDR 的传感距离。广东工业大学研究团队^[65]近期提出的光谱拼接法(SSM)揭示并克服了相位噪声对其的限制,将 OFDR 的传感距离突破 1 km。

考虑相位噪声作用时,解调得到的应变表示为

$$\epsilon = \frac{\Delta\varphi_{\text{shf}} + e_s(t)}{\rho_\epsilon f_0 \tau}, \quad (13)$$

式中: $\Delta\varphi_{\text{shf}}$ 为应变引入的相移; ρ_ϵ 为应变系数; f_0 为初始频率。

OFDR 采用的宽谱扫描问询光带来了优异传感性能,但也带来了更大的相位噪声;校正算法需要同时面对巨大非线性相位以及光源相位噪声。非线性扫频校正算法难以在长距离下精细补偿相位噪声,而适用于长距离传感的 PNC^[84]、去斜滤波器^[85]等算法也不能很好地校正大幅度扫频非线性。SSM 方法对宽谱扫描信号进行细分,降低了单一片段的非线性相位噪声,使其适配去斜滤波算法^[56]的补偿能力;在抑制每个片段的相位噪声后,再进行频谱拼接以恢复完整的频谱信息。SSM-OFDR 取得的效果如图 15 所示,在 20 nm 扫频范围下实现了 1170 m 光纤的分布式应变解调,具有 1 cm 的空间分辨率与 $\pm 1.1 \mu\epsilon$ 的应变精度,应变解调范围能达到 10000 $\mu\epsilon$ 。

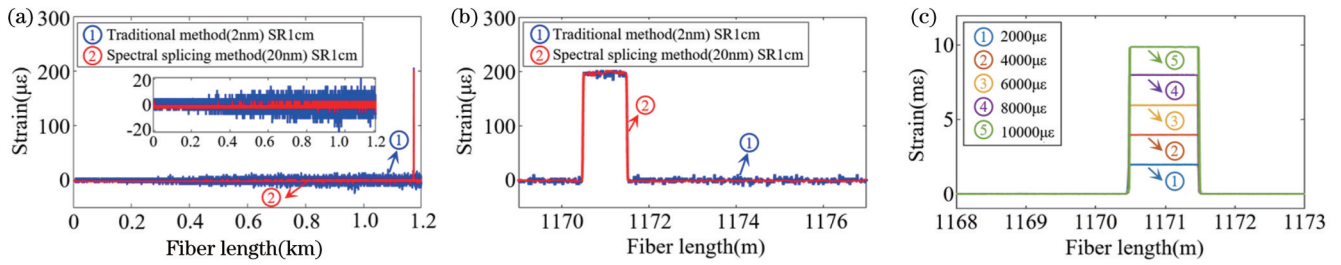


图 15 SSM-OFDR 应变测试结果^[65]。(a)光谱拼接前后结果;(b)特写视角;(c)大应变测量

Fig. 15 Strain measuring results by SSM-OFDR^[65]. (a) Results before and after spectral splicing; (b) close-up view; (c) large strain measuring

4.3.3 OFDR 传感量限扩展

OFDR 的实际应变测量范围会受到距离模糊与光谱失配的影响。距离模糊原理如图 16(a)所示,外界温度/应变带来了光纤光程变化,导致 RBS 信息错位,当累积的错位超过空间分辨率时将无法解调应变^[114]。类似的错

位还体现在光谱上,如图 16(b)所示,温度/应变大小与光谱偏离量成正比,互相关信噪比在光谱偏离超过 20% 的扫频范围时出现明显的退化^[101],即温度/应变高精度传感的量限约为理论值的 20%。高精度的距离模糊校正与光谱失配抑制是实现大应变解调的重要前提。

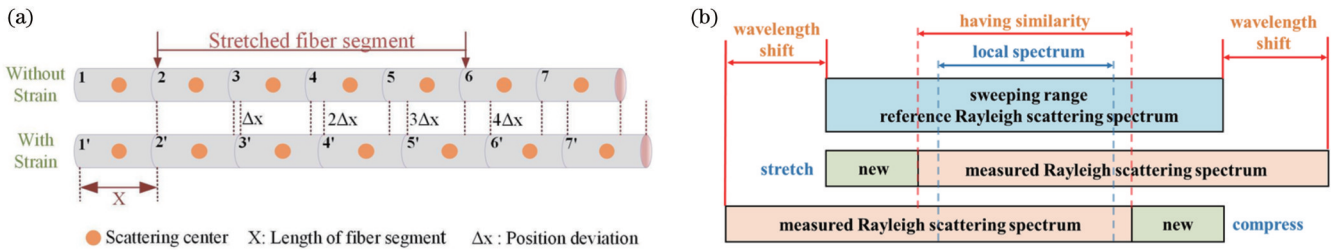


图 16 应变导致距离模糊与光谱失配现象示意图^[101,114]。(a)距离模糊原理;(b)光谱失配原理

Fig. 16 Schematic illustrations of range ambiguity and spectral mismatch caused by strain^[101,114]. (a) Principle of range ambiguity; (b) principle of spectral mismatch

光谱失配问题在 2018 年被认识到,为此, Feng 等^[101]提出了局部互相关法来改善大应变造成的整体相关性退化问题,该方法后续发展为光谱配准法^[92]、零均值归一化互相关^[102]等衍生技术,实现了最大 10000 $\mu\epsilon$ 的解调。该算法的流程如图 17(a)所示,将截取的局部传感光谱信息与整段的参考光谱进行互相关,避免了失配部分光谱带来的互相关噪声与伪峰。光谱配准法在局部互相关的基础上,对参考光谱也添加了

约束条件,进一步抑制了干扰噪声,并提高了解调速度。

针对距离模糊问题的位置补偿方法在 2019 年由 Zhao 等^[92]提出,该方法是基于闭环反馈的思想实现的,具体为:通过前端空间位置已解调的分布式应变计算累积的光程偏离量,并反馈修正下一空间位置的数据窗口位置。典型的位置补偿方法的工作流程如图 17(b)所示。在后续发展中,该方法能够在 2 mm 空间

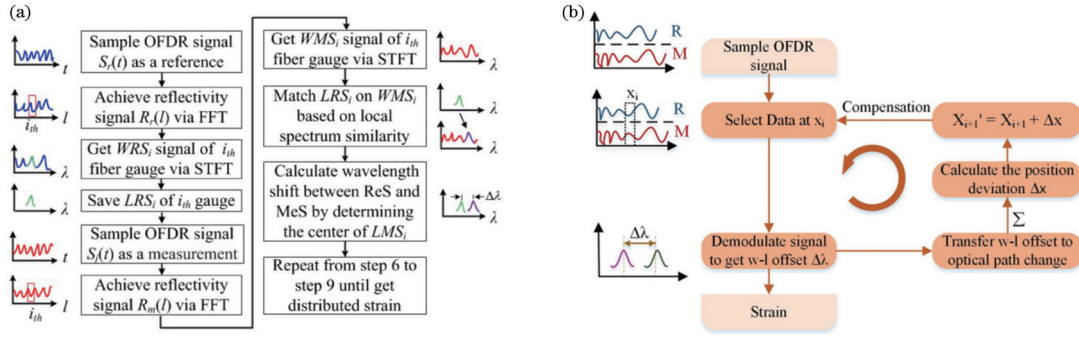


图 17 算法工作流程^[101,114]。(a)局部互相关;(b)位置补偿

Fig. 17 Algorithmic workflow^[101,114]. (a) Local inter-correlation; (b) position compensation

分辨率下实现 10000 $\mu\epsilon$ 的解调^[98]。此外,根据 30 cm 的应变作用长度可推算应变导致光纤拉伸 3 mm,超出 2 mm 的空间分辨率,这说明位置补偿是大应变解调的必要条件,补偿的精度可以达到亚 mm 级。

4.3.4 OFDR 传感精度提升

由图 10 可知,在距离模糊、光谱失配被充分校正的前提下,限制应变测量精度的因素主要是 RBS 畸变,具体包括非线性相位噪声、偏振噪声等。目前的精度提升方法主要有两条路线:1)针对 RBS 光谱质量进行优化,诸如非线性相位噪声抑制^[73]、光谱拼接^[65]、使用散射增强光纤^[115]等方法;2)针对解调过程或解调结果的降噪优化,如谱域插值^[116]、图像降噪^[117-119]、小波降噪^[120]等技术。RBS 信号质量是高精度解调的重要前提,在本文其他部分已有所提及,此处主要介绍降噪技术在 OFDR 中的应用。以光纤长度为横轴、光谱偏移为纵轴、互相关强度为竖轴,可构造一幅 RBS 信息的三维图像,分布式应变将以互相关峰值的形式绘制在

图像中。去除图像噪点等效于去除互相关伪峰与噪声,可以提升应变解调精度。这一思想最早于 2020 年由 Zhao 等^[117]提出,之后他们陆续提出了总变分法、平方图像格式、非局部均值算法、二维高斯滤波等三维图像降噪方法。2022 年, Pan 等^[119]提出 BM3D-SAPCA (block-matching three-dimensional shape-adaptive principal component analysis) 算法,通过堆叠三维特征图像多维地交叉比较图像中的冗余与噪声,实现了进一步降噪,算法的工作流程如图 18 所示。图像处理主要作用于互相关过程中的加性白噪声,目前图像处理方法能显著地将应变测量精度提升 4~5 倍,一个典型的结果是在 5 cm 空间分辨率下使用 BM3D-SAPCA 算法将应变精度从 1.52 $\mu\epsilon$ 提升至 0.31 $\mu\epsilon$ 而不影响其他指标。OFDR 中各种噪声与非理想因素均能在一定程度上转为互相关噪声。图像处理方法能够被扩展用于解决相位噪声、环境噪声等多种问题,但其主要的代价是更高的计算量与更长的数据处理时间。

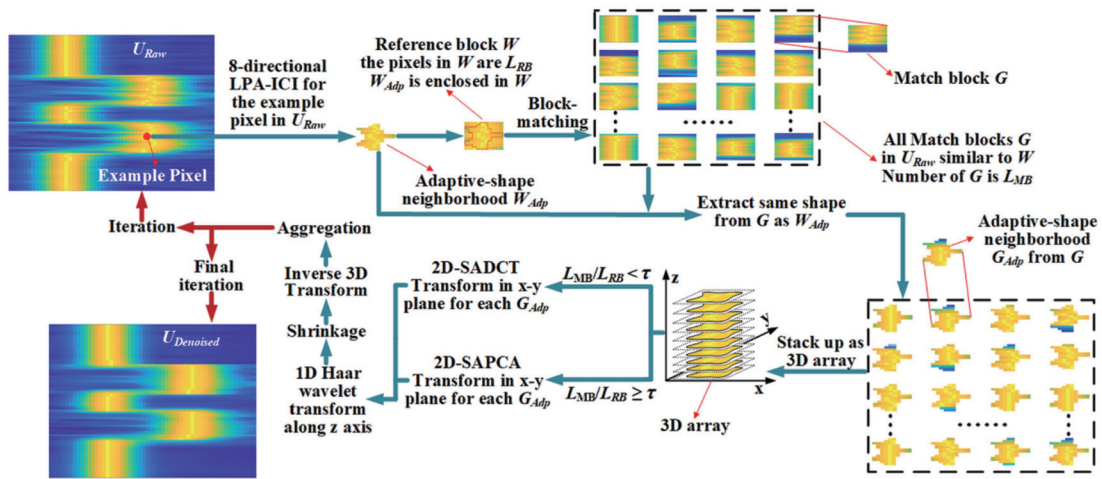


图 18 BM3D-SAPCA 算法的工作流程^[119]

Fig. 18 Workflow of the BM3D-SAPCA algorithm^[119]

4.3.5 OFDR 频率响应提升技术

应变频率响应与幅值范围存在硬件瓶颈制约,原因是:幅值范围需要扫描很宽的光谱范围来保证,宽谱、高重复频率的扫描需求意味着极高的扫频速率,这

对于激光器来说是难以兼顾的,同时这也提高了对采集和探测电路硬件带宽的要求。相位解调法(TGD-OFDR、 Φ -OFDR)的单次测量幅值范围受解调机理的限制,通常使用窄谱询问光,采用频分复用等方法扩展

频率响应^[17]。光谱解调法难以实现动态快速测量,目前通过调控参数、GPU 加速运算等方式突破性地实现了 100 Hz、±200 με 的振动信号测量;若幅值范围提升至 -1000~1000 με,可测频率将会降低至 20 Hz^[92]。上述报道中所使用的扫频范围达到了 2000 nm/s,这带来了极高的硬件带宽。

广东工业大学杨军教授团队提出了光谱游标技术(SV-OFDR),它有效切断了频率响应与幅值范围之

间的约束关系。如图 19 所示,SV-OFDR 使用了两种光源调制模式:参考的宽带 RBS 光谱(调频范围: $f_{R-sta} \sim f_{R-end}$)由 TLS 的内调制模式测量获得,以构造“主尺”,保证应变量程;窄带 RBS 光谱(调频范围: $f_{S-sta} \sim f_{S-end}$)充当“游标”,通过高重复频率的啁啾脉冲进行测量。解调时,以 RBS 光谱为刻度,将“游标”在“主尺”上滑动相关搜索游标位置 f_{Ref} 与 f_{Sen} ,通过波长偏移量 Δf 即可获得分布式应变信息。

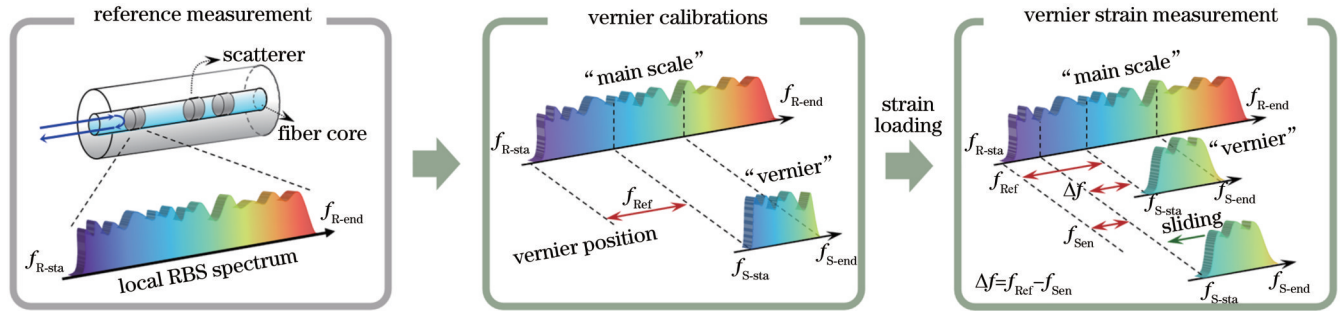


图 19 SV-OFDR 的解调原理
Fig. 19 Demodulation principles of SV-OFDR

如图 20 所示,SV-OFDR 的最大可测应变为 10856 με,应变量程内线性度为 99%,重复性为 0.4 με [3σ(高斯分布法则)],频率响应为 1.21 kHz,灵敏度为 18.7 ne/√Hz。SV-OFDR 以散射光谱特征为纽带,融

合了宽谱扫描与时间门控调制的技术优势,保留了 OFDR 大应变、高精度的静态技术特征,具备实现长距离动态测试的技术潜质。

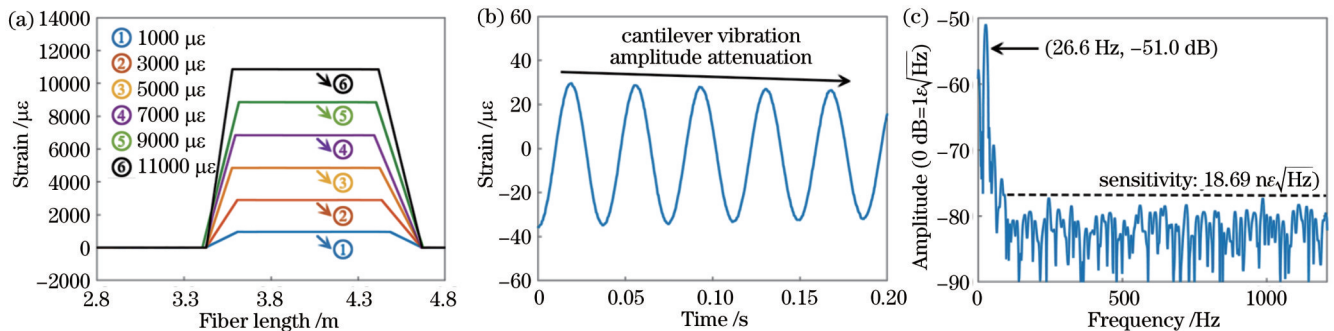


图 20 SV-OFDR 分布式应变测试结果。(a) 超大应变解调结果;(b)(c) 振动信号解调结果
Fig. 20 SV-OFDR distributed strain measuring results. (a) Large strain demodulation results; (b)(c) vibration signal demodulation results

5 高性能 OFDR 测试与传感应用

近些年,在光纤及器件测试、链路故障诊断、油气开采与运输监测、海洋勘探等重大需求的牵引下,国内外已研发了多种 OFDR 测试仪器与传感解调仪,并形成了大量的应用场景与案例。接下来将概述 OFDR 仪器发展现状,并列举测试与传感应用领域的典型案例。

5.1 国内外 OFDR 仪器简介

国外 OFDR 仪器设备的研发起步较早,如表 6 所示,2003 年美国 Luna 公司推出了首台 OFDR 仪器 OBR-4600,该仪器具有百 m 级的 RBS 测试长度与 20 μm 的空间分辨率,测试长度最长可达 2 km(1 mm

空间分辨率),成为高精度链路、光纤器件、系统光路检测必不可少的设备。2005 年 Luna 公司为 OBR-4600 增加了温度/应变传感功能,并于 2010 年推出了 ODiSI-6000 系列动态应变仪,该系列仪器所实现的传感距离均在百 m 内,其特色是 mm 级高空间分辨率与 με 级精度两项核心指标。日本 Santec 公司也在 2022 年推出了 SPA-100 散射测试仪,该仪器在空间分辨率上具有优势。

国内 OFDR 仪器开发相比国外落后 10 余年,虽然已研发出基于 OFDR 的光纤分布式散射测量仪和光纤传感分布式解调仪,但目前国内应用仍以国外进口仪器为主,国产替代与应用规模均较低,这是目前的痛

表 6 OFDR 仪器性能对比
Table 6 Performance comparison of OFDR instruments

Type	Country	Maker	Model	Length	Spatial resolution	Amplitude		Measuring rate		
						Range	Accuracy			
RBS	USA	Luna Inc.	OBR-4600	70 m	20 μm	80 dB	-130 dB	3 s		
				2 km	1 mm	60 dB				
	China	Mega-Sense Co.	OCI	Jun Long	OFDR	120 m	5 mm	65 dB	-65 dB	15 s
				BACIRI	OFFD-L-2502	25 m	2 mm	50 dB	-120 dB	1 s
				GDUT	OFDR-D	100 m	20 μm	80 dB	-130 dB	12 s
				GDUT	OFDR-D	100 m	20 μm	90 dB	-135 dB	5 s
				GDUT	OFDR-F	5 km	0.5 mm	70 dB	-130 dB	10 s
Japan	Santec	SPA-100	4.5 m	6 μm	70 dB	-135 dB	5 s			
Sensing	USA	Luna Inc.	OBR-4600	70 m	1 cm	$\pm 15000 \mu\epsilon$	$\pm 1 \mu\epsilon$	3 s		
				ODiSI-6000	20 m	0.65 mm	$\pm 15000 \mu\epsilon$	$\pm 5 \mu\epsilon$	12.5 Hz	
					100 m	2.6 mm	$\pm 15000 \mu\epsilon$	$\pm 2 \mu\epsilon$	10 Hz	
	China	Mega-Sense Co.	OCI	OSI-S	100 m	1 mm (min)	$\pm 12000 \mu\epsilon$	$\pm 1 \mu\epsilon$	—	
				OSI-D	20 m	0.65 mm	$\pm 12000 \mu\epsilon$	$\pm 4 \mu\epsilon$	50 Hz	
				GDUT	OFDS-H	100 m	2 mm	$\pm 12000 \mu\epsilon$	$\pm 2 \mu\epsilon$	8 s
					OFDS-S	5 km	5 cm	$\pm 12000 \mu\epsilon$	$\pm 0.5 \mu\epsilon$	30 s

点之一。

在 OFDR 测试仪器方面：2014 年，江苏骏龙光电科技股份有限公司在国内首次推出 OFDR 仪器。2019 年武汉昊衡科技有限公司 (Mega-Sense Co.) 推出 OCI 散射测试仪，该仪器的各项指标达到了 OBR-4600 水平，且将测量距离扩展至 100 m，但其测试时间有所损失。此外，北京航天控制仪器研究所 (BACIRI)、广东工业大学 (GDUT) 也推出了自研的 OFDR 仪器，包括全面对标 OBR-4600 的 OFDR-D 与 OFDR-F，它们在测量距离、空间分辨率、动态范围方

面具有优势，如表 6 所示。

在 OFDR 传感解调仪方面：国内的主要仪器是由武汉昊衡科技有限公司和广东工业大学推出的，如图 21 所示。武汉昊衡科技有限公司推出的 OSI-S 与 OSI-D 分别对标 OBR-4600 与 ODiSI-6000，基本实现指标覆盖。广东工业大学推出的 OFDS-H 与 OFDS-S 型应变解调仪的特色是将传感距离扩展到 5 km 以上，是目前传感距离最长的 OFDR 仪器，可应用于油气勘探、智能结构监测以及光纤陀螺环检测等长距离高精度传感应用领域。



图 21 典型 OFDR 仪器。(a) Luna OBR-4600; (b) 武汉昊衡科技有限公司 LGA50; (c) 广东工业大学 OFDS
Fig. 21 Typical OFDR instruments. (a) Luna OBR-4600; (b) Mega-Sense Co. LGA50; (c) GDUT OFDS

5.2 高精度分布式测试应用举例

OFDR 技术能够精细地获取光纤/光波导沿线的散射、反射、偏振等特征信息，进而反演待测光纤链路/器件的传输特性、缺陷故障等，具体包括：传输损耗、异常反射、熔接事件、外破断点、过量弯曲以及易损腐蚀等情况^[121]。基于上述优势与测试能力，OFDR 分布式测试仪被广泛应用于光纤筛选、光纤链路/通信网络监测^[122-123]、多芯^[124]/空芯^[125]/保偏^[126]等普通和特种光纤等长距离、高精度测试场合以及耦合器等光无源器件^[127]、集成光波导^[12,128]、硅光集成芯片^[129-130]等大动态、

高分辨测试场合，已经成为一种不可替代的高精度检测手段，对光纤及器件的参数测试、质量检验、缺陷评估与工艺迭代具有重要意义。围绕 OFDR 光纤与器件两类主要的测试需求，分别列举了两项典型的超高性能 OFDR 应用案例。

应用案例之一是在超长距离、超高精度的光纤及光纤链路/网络测试方面。如图 22 所示，北京理工大学董毅教授团队^[55]提出高阶光锁相 OFDR，在 242 km 超长距离下实现了 4.3 cm 空间分辨率，是目前测量距离最长的 OFDR，已经能够满足海缆单跨、陆缆监测的

测试需求,能够对光缆进行物理层检测,检测参量包括 故障点、故障原因、线缆损耗等。

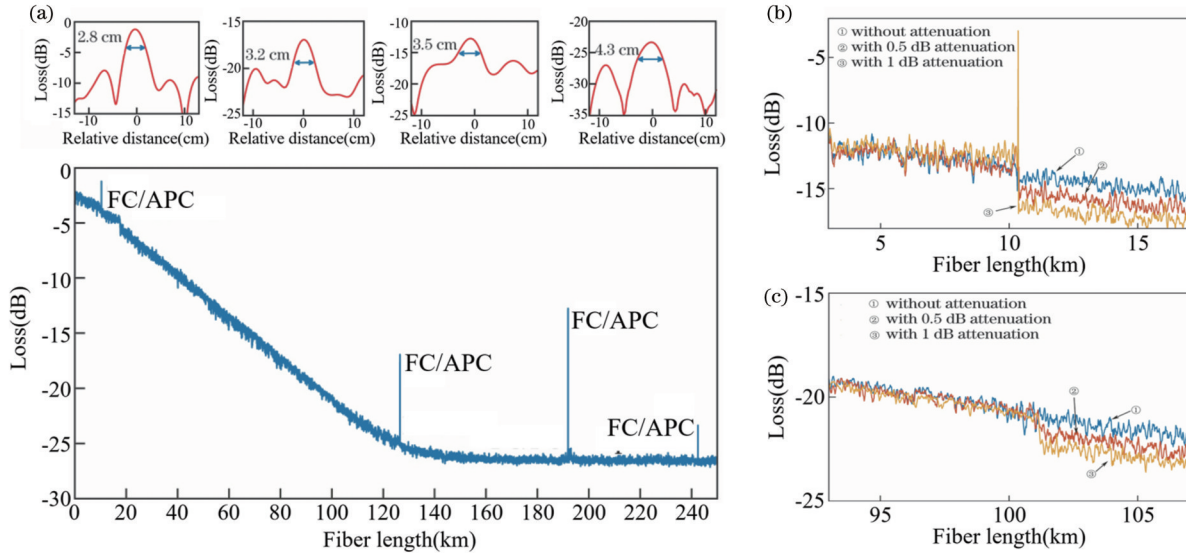


图 22 超长距离光纤与链路测试应用^[55]。(a)光锁相控制的 OFDR 所测得的光纤链路损耗;(b)(c)10 km 与 100 km 处光纤损耗测量精度

Fig. 22 Ultra-long distance optical fiber and link measuring application^[55]. (a) Fiber link loss of OFDR controlled by optical phase locking; (b)(c) measurement accuracies of optical fiber loss at 10 km and 100 km

应用案例之二是在超高精度分辨、超大动态测量范围的光无源器件、光芯片测试方面。如图 23(a)、(b)所示,日本横滨国立大学研究团队^[129]使用 OFDR 技术对硅光子集成电路进行分析,对激光雷达芯片内部线波导、光开关等的反射和损耗进行探测,最终的空间分辨率优于 2.5 μm ,实现了芯片上各组件的光学特性评估。如图 23(c)、(d)所示,广东工业大学杨军教授团队^[42]提出的光频域透反射测试仪/偏振与反射询问仪

(OFDR/P)能够以 10 $\mu\text{m}/8\text{ cm}$ 反射/透射空间分辨率、-140 dB/-110 dB 反射/透射灵敏度、100 dB 动态范围的超高性能对器件、波导的内部结构、核心指标、工艺过程、故障缺陷进行超精细测量与表征。OFDR/P 已应用于光纤耦合器、Y 波导调制器、各类直波导调制器、新型光纤样品等高性能光纤与器件的质量测试与工艺迭代,对光纤陀螺、光纤水听器为代表的高精度光学系统的性能提升有重要意义。

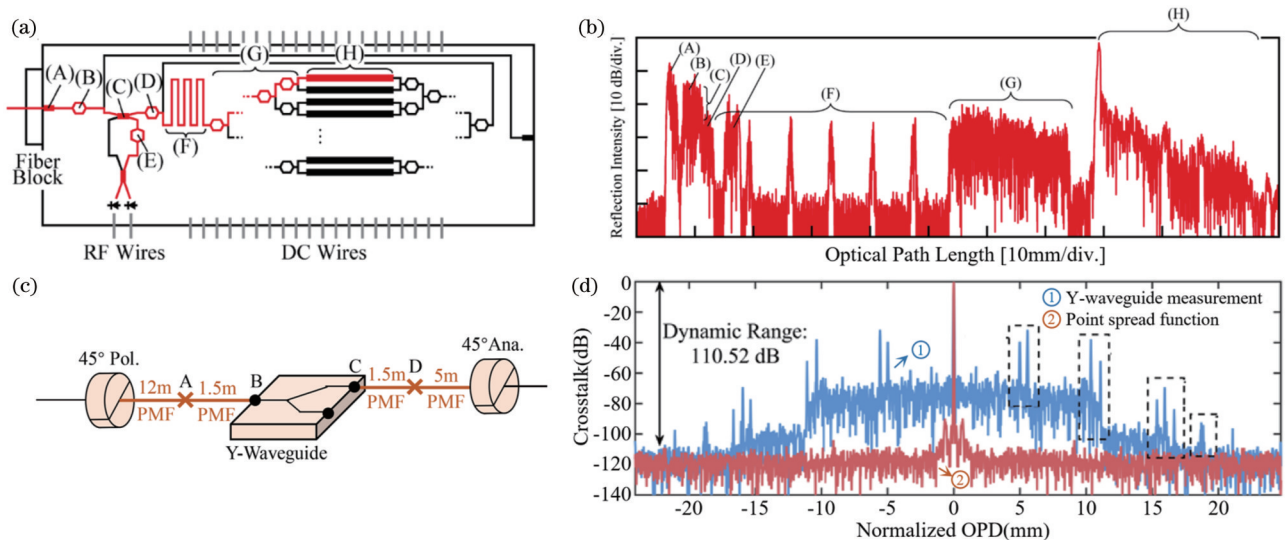


图 23 超高精度光芯片测试应用。(a)(b)制备的 LiDAR 芯片及其测量的反射谱($\Delta R=10\ \mu\text{m}/\text{ng}$)^[129]; (c)(d)Y 波导和分布式偏振串扰测量结果^[42]

Fig. 23 Ultra-high precision optical chip measuring applications. (a)(b) Fabricated LiDAR chip and measured reflection spectrum, where $\Delta R=10\ \mu\text{m}/\text{ng}$ ^[129]; (c)(d) Y-waveguide and distributed polarization crosstalk measurement results^[42]

5.3 高性能分布式传感应用举例

超长距离、超高精度是 OFDR 传感技术的标签,它能够在近百 km 长度范围内感知光纤受到的微小应变、声波振动、温度变化^[131-133];也能以 mm 级空间分辨率应对三维形状反演、三维结构识别^[134-135]等精细传感场合;此外,它结合其他特殊解调方法或增敏结构还能实现 10 余种物理量、生化量传感^[64]。目前,基于 OFDR 的分布式传感技术被广泛应用在水下目标探测^[136]、地震海啸预测^[137]、油气井下温压监测^[138]、高压电网温压检测^[139]等场合,为海洋、高压、电磁等极端环境提供超长距离的温度、气压监测。此外,它还能够可在可变翼飞行器^[140]、风电叶轮形变^[141]等结构监测场合进行精细的应变监测与形状传感。

高性能 OFDR 传感的典型应用之一是由上海交通大学何祖源教授团队^[142]提出的超长距离 TGD-OFDR 技术与研制的仪器 HiFi-DAS。HiFi-DAS 能够

实现最长 108 km 的传感距离并保持 5 m 的空间分辨率,其振动测试带宽可达 10 kHz。HiFi-DAS 已经在周界入侵、油气管道安全、煤矿安全、海洋水声侦听、城市物探、轨道交通安全等领域取得大量应用^[138],对民生、营生安全意义重大,如图 24 所示。

高性能 OFDR 传感的典型应用之二是光纤精细应变测量与结构反演。光纤缠绕结构是一种典型的超精细且高度复杂的结构,如,光纤陀螺敏感环。广东工业大学杨军教授团队进行了大量的全温内应力测试与结构模型建立工作,所使用的高性能 OFDR 能够以 5 cm 空间分辨率实现 3 km 以上长度光纤的大应变测量,应变精度达到 $\pm 1.2 \mu\epsilon$,温度精度达到 $\pm 0.5 \text{ }^\circ\text{C}$ 。当其应用于光纤陀螺环测试时,可清晰地获得光纤环内换层、换匝的精细应力特征,如图 25 所示,该高性能 OFDR 已经在光纤敏感环的绕制工艺提升、光纤陀螺的性能优化方面表现出巨大潜力^[143]。

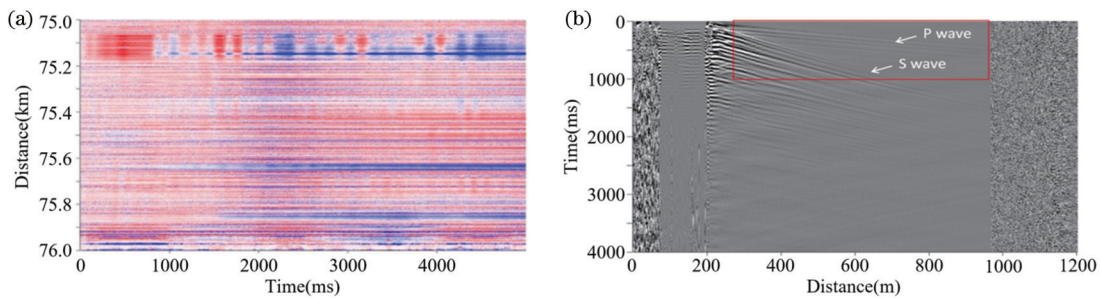


图 24 分布式声波传感典型应用^[138]。(a)长期深海海底观测站观测到的声学信号;(b)测量到的地震波剖面图

Fig. 24 Typical application of distributed acoustic sensing^[138]. (a) Observed acoustic signal in long-term deep sea floor observatory; (b) measured seismic profiles of the surface wave

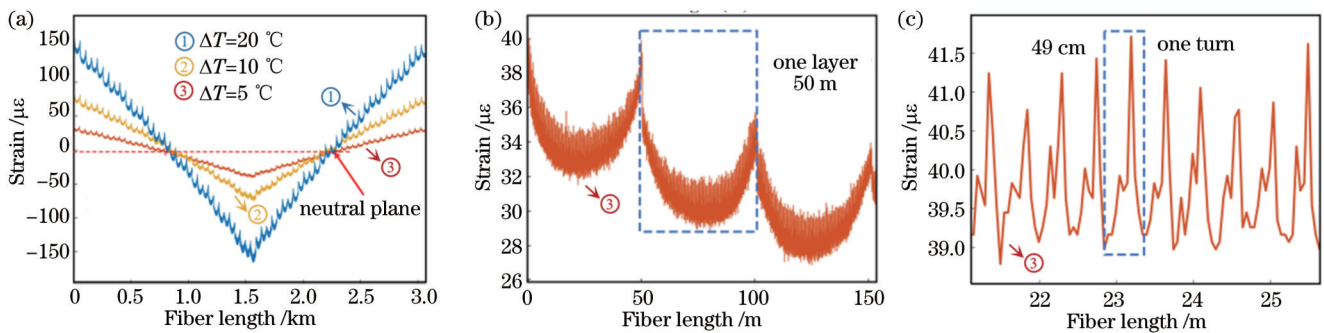


图 25 3 km 光纤环应变测试结果。(a)不同温度激励下的应变结果;(b)层间应变;(c)匝间应变

Fig. 25 3 km fiber coil strain measurement results. (a) Strain results under different temperature excitations; (b) interlayer strain; (c) interturn strain

6 结束语

自 1981 年始,OFDR 技术已历经了 42 年的发展,在高性能光纤器件测试、高精度多参量光纤传感等领域取得了广泛的应用。在国内,近 10 年来,我国在 OFDR 理论创新与技术研发方面基本追平了美国、日本等发达国家,整体水平实现了与发达国家“并跑”;并且在 OFDR 测试与传感的最长距离、空间分辨率、测

量容量、传感范围等技术指标方面实现了超越,优于国外研究。其不足之处在于 OFDR 技术的典型应用领域与场景还需不断拓展,技术优势与应用效果还需精耕细作并持续凸显。

未来,随着高精度光纤与器件性能的不不断提升以及分布式高性能传感应用场景与需求的不断扩展,要求 OFDR 技术的测量性能更高、环境适应性更强、应用领域更加多元、测试性价比更高。因此,其潜在的研

究方向包括:

1)从技术内在发展与推动的角度出发,其一,多域定位(时、频、相干域)、多维调制(幅度、相位、偏振调制)、多域解调(RBS相位、RBS光谱域)的复合调制技术,包括已经发展的时频复合域TGD-OFDR,双调制模式复合SV-OFDR等,或许是突破测量极限、实现超高性能OFDR技术的重要途径;其二,多参量解耦/交耦参量脱敏的高精度OFDR传感技术应该得到重视,特别是如何克服OFDR传感固有的非特异性缺陷,实现精度与抗干扰能力的提升;其三,关注人工智能与先进算法的赋能作用,提升噪声抑制能力与解调精度,并保证解算时效;其四,发展OFDR核心器件与光路的片上集成以及光源、探测器与光电芯片的混合集成技术,实现小体积、低功耗、低成本的OFDR仪器和核心模块。

2)从重大需求与应用牵引的角度出发,其一,面向国家重大需求,推动OFDR技术自主可控与硬件国产化,其核心难点包括连续无跳模的可调谐激光源、高速高精度光电转换与数据采集模块等;其二,提升OFDR的环境适应性,包括测量仪器与解调的抗振动干扰性能,以确保分布式测试与传感核心技术指标在不同场景下不退化,使OFDR技术从实验室测量逐步走向户外的工程应用;其三,面向军用器件测试、油气资源勘探、电力能源监测等重大需求,进一步加强核心领域和典型场景的应用开发,提出分布式高性能专用化测试与定量化传感方法,为特殊应用场景开发定制化软件,打通OFDR技术应用的“最后一公里”。

参 考 文 献

- [1] Hartog A H. An introduction to distributed optical fiber sensors [M]. Boca Raton: CRC Press, 2016.
- [2] Derickson D J. Fiber optic test and measurement[M]//Upper Saddle River. 1998. <https://www.semanticscholar.org/paper/Fiber-optic-test-and-measurement-Derickson/b946ed3aa6101c5b0f5867e400d305d25bbac748>.
- [3] 廖延彪,黎敏,张敏. 光纤传感技术与应用[M]. 北京:清华大学出版社,2009.
Liao Y B, Li M, Zhang M. Optical fiber sensing techniques and applications[M]. Beijing: Tsinghua University Press, 2009.
- [4] 张旭苹. 全分布式光纤传感技术[M]. 北京:科学出版社,2013.
Zhang X P. Fully distributed optical fiber sensing technology [M]. Beijing: Science Press, 2013.
- [5] Lopez-Higuera J M, Cobo L R, Incera A Q, et al. Fiber optic sensors in structural health monitoring[J]. Journal of Lightwave Technology, 2011, 29(4): 587-608.
- [6] Nokes G. Optimising power transmission and distribution networks using optical fibre distributed temperature sensing systems[C]//IEE Seminar on Asset Management of Cable Systems, February 3, 2000, Brimingham, UK. London: IET Press, 2000: 4/1-4/9.
- [7] Glisic B, Yao Y. Fiber optic method for health assessment of pipelines subjected to earthquake-induced ground movement[J]. Structural Health Monitoring, 2012, 11(6): 696-711.
- [8] Adachi S. Distributed optical fiber sensors and their applications [C]//2008 SICE Annual Conference, August 20-22, 2008, Chofu, Japan. New York: IEEE Press, 2008: 329-333.
- [9] Sladen A, Rivet D, Ampuero J P, et al. Distributed sensing of earthquakes and ocean-solid Earth interactions on seafloor telecommunication cables[J]. Nature Communications, 2019, 10: 5777.
- [10] Williams E F, Fernández-Ruiz M R, Magalhaes R, et al. Distributed sensing of microseisms and teleseisms with submarine dark fibers[J]. Nature Communications, 2019, 10: 5778.
- [11] von der Weid J P, Passy R, Mussi G, et al. On the characterization of optical fiber network components with optical frequency domain reflectometry[J]. Journal of Lightwave Technology, 1997, 15(7): 1131-1141.
- [12] Glombitza U, Brinkmeyer E. Coherent frequency-domain reflectometry for characterization of single-mode integrated-optical waveguides[J]. Journal of Lightwave Technology, 1993, 11(8): 1377-1384.
- [13] Soller B J, Gifford D K, Wolfe M S, et al. High resolution optical frequency domain reflectometry for characterization of components and assemblies[J]. Optics Express, 2005, 13(2): 666-674.
- [14] Hu Z H, Wang B J, Wang L S, et al. Improving spatial resolution of chaos OTDR using significant-bit correlation detection[J]. IEEE Photonics Technology Letters, 2019, 31(13): 1029-1032.
- [15] Denisov A, Soto M A, Thévenaz L. Going beyond 1000000 resolved points in a Brillouin distributed fiber sensor: theoretical analysis and experimental demonstration[J]. Light: Science & Applications, 2016, 5(5): e16074.
- [16] Wang B, Fan X Y, Fu Y X, et al. Enhancement of strain/temperature measurement range and spatial resolution in Brillouin optical correlation domain analysis based on convexity extraction algorithm[J]. IEEE Access, 2019, 7: 32128-32136.
- [17] He Z Y, Liu Q W. Optical fiber distributed acoustic sensors: a review[J]. Journal of Lightwave Technology, 2021, 39(12): 3671-3686.
- [18] Healey P. Optical time domain reflectometry: a performance comparison of the analogue and photon counting techniques[J]. Optical and Quantum Electronics, 1984, 16(3): 267-276.
- [19] Eickhoff W, Ulrich R. Optical frequency-domain reflectometry in single-mode fibers[C]//Integrated Optics and Optical Fiber Communication, April 27-29, 1981, San Francisco, California. Washington, DC: OSA, 1981: WF3.
- [20] Youngquist R C, Carr S, Davies D E N. Optical coherence-domain reflectometry: a new optical evaluation technique[J]. Optics Letters, 1987, 12(3): 158-160.
- [21] Wang A B, Wang Y C. Chaos correlation optical time domain reflectometry[J]. Science China Information Sciences, 2010, 53(2): 398-404.
- [22] Juarez J C, Taylor H F. Field test of a distributed fiber-optic intrusion sensor system for long perimeters[J]. Applied Optics, 2007, 46(11): 1968-1971.
- [23] Li J, Gan J L, Zhang Z S, et al. High spatial resolution distributed fiber strain sensor based on phase-OFDR[J]. Optics Express, 2017, 25(22): 27913-27922.
- [24] Davé D P, Milner T E. Optical low-coherence reflectometer for differential phase measurement[J]. Optics Letters, 2000, 25(4): 227-229.
- [25] Wang S, Fan X Y, Liu Q W, et al. Distributed fiber-optic vibration sensing based on phase extraction from time-gated digital OFDR[J]. Optics Express, 2015, 23(26): 33301-33309.
- [26] Pastor-Graells J, Martins H F, Garcia-Ruiz A, et al. Single-shot distributed temperature and strain tracking using direct detection phase-sensitive OTDR with chirped pulses[J]. Optics Express, 2016, 24(12): 13121-13133.
- [27] Nakazawa M, Tokuda M, Negishi Y. Measurement of polarization mode coupling along a polarization-maintaining optical fiber using a backscattering technique[J]. Optics Letters, 1983, 8(10): 546-548.

- [28] Larin K V, Akkin T, Esenaliev R O, et al. Phase-sensitive optical low-coherence reflectometry for the detection of analyte concentrations[J]. *Applied Optics*, 2004, 43(17): 3408-3414.
- [29] Dakin J P, Pratt D J, Bibby G W, et al. Temperature distribution measurement using Raman ratio thermometry[J]. *Proceedings of SPIE*, 1986, 0566: 249-256.
- [30] Geng J P, Xu J D, Li Y, et al. The development of the model and arithmetic for the fully distributed fiber optic sensor based on Raman optical-fiber frequency-domain reflectometry (ROFDR) [J]. *Sensors and Actuators A: Physical*, 2002, 101(1/2): 132-136.
- [31] Li J, Wang C Y, Cao K Y, et al. Breakthrough the physical barrier on spatial resolution in Raman distributed fiber sensing using chaotic correlation demodulation[J]. *APL Photonics*, 2023, 8(7): 076105.
- [32] Tsai S C, Huang M H, Chen Y K. Stimulated Raman scattering-induced baseband video distortion due to 1.65- μm OTDR online monitoring in 1.55- μm AM-VSB CATV system [J]. *IEEE Photonics Technology Letters*, 2002, 14(7): 1016-1018.
- [33] Shimizu K, Horiguchi T, Koyamada Y, et al. Coherent self-heterodyne Brillouin OTDR for measurement of Brillouin frequency shift distribution in optical fibers[J]. *Journal of Lightwave Technology*, 1994, 12(5): 730-736.
- [34] Minardo A, Bernini R, Ruiz-Lombera R, et al. Proposal of Brillouin optical frequency-domain reflectometry (BOFDR) [J]. *Optics Express*, 2016, 24(26): 29994-30001.
- [35] Mizuno Y, He Z Y, Hotate K. Enlargement of measurement range of Brillouin optical correlation-domain reflectometry based on temporal gating scheme[C]//2008 34th European Conference on Optical Communication, September 21-25, 2008, Brussels, Belgium. New York: IEEE Press, 2008.
- [36] Ma Z, Zhang M J, Liu Y, et al. Incoherent Brillouin optical time-domain reflectometry with random state correlated Brillouin spectrum[J]. *IEEE Photonics Journal*, 2015, 7(4): 6100407.
- [37] Horiguchi T, Kurashima T, Tateda M. Tensile strain dependence of Brillouin frequency shift in silica optical fibers[J]. *IEEE Photonics Technology Letters*, 1989, 1(5): 107-108.
- [38] Garus D, Gogolla T, Krebber K, et al. Distributed sensing technique based on Brillouin optical-fiber frequency-domain analysis[J]. *Optics Letters*, 1996, 21(17): 1402-1404.
- [39] Song K Y, He Z Y, Hotate K. Distributed strain measurement with millimeter-order spatial resolution based on Brillouin optical correlation domain analysis and beat lock-in detection scheme [C]//Optical Fiber Sensors, October 23-27, 2006, Cancún, Mexico. Washington, DC: OSA, 2006: ThC2.
- [40] Wang Y H, Zhang M J, Zhang J Z, et al. Millimeter-level-spatial-resolution Brillouin optical correlation-domain analysis based on broadband chaotic laser[J]. *Journal of Lightwave Technology*, 2019, 37(15): 3706-3712.
- [41] Huang Z J, Wu C Q, Wang Z, et al. Distributed measurement of polarization mode coupling in fiber ring based on P-OTDR complete polarization state detection[J]. *Optics Express*, 2018, 26(4): 4798-4806.
- [42] Yu Z J, Zhuang Q Q, Lin Y, et al. Optical frequency domain polarimetry for distributed polarization crosstalk measurement beyond a 110 dB dynamic range[J]. *Optics Letters*, 2022, 47(16): 4271-4274.
- [43] Takada K, Noda J, Okamoto K. Measurement of spatial distribution of mode coupling in birefringent polarization-maintaining fiber with new detection scheme[J]. *Optics Letters*, 1986, 11(10): 680-682.
- [44] Shelby R M, Levenson M D, Bayer P W. Resolved forward Brillouin scattering in optical fibers[J]. *Physical Review Letters*, 1985, 54(9): 939-942.
- [45] Chow D M, Soto M A, Thévenaz L. Frequency-domain technique to measure the inertial response of forward stimulated Brillouin scattering for acoustic impedance sensing[J]. *Proceedings of SPIE*, 2017, 10323: 1032311.
- [46] Song K Y, Zou W, He Z, et al. All-optical dynamic grating generation based on Brillouin scattering in polarization maintaining fiber[J]. *Optics Letters*, 2008, 33(9): 926-928.
- [47] Marie T F B, Yang B, Han D Z, et al. Principle and application state of fully distributed fiber optic vibration detection technology based on Φ -OTDR: a review[J]. *IEEE Sensors Journal*, 2021, 21(15): 16428-16442.
- [48] Barnoski M K, Jensen S M. Fiber waveguides: a novel technique for investigating attenuation characteristics[J]. *Applied Optics*, 1976, 15(9): 2112-2115.
- [49] Qin J, Zhang L, Xie W L, et al. Ultra-long range optical frequency domain reflectometry using a coherence-enhanced highly linear frequency-swept fiber laser source[J]. *Optics Express*, 2019, 27(14): 19359-19368.
- [50] Qu S, Xu Y P, Huang S, et al. Recent advancements in optical frequency-domain reflectometry: a review[J]. *IEEE Sensors Journal*, 2023, 23(3): 1707-1723.
- [51] Ahn T J, Lee J Y, Kim D Y. Suppression of nonlinear frequency sweep in an optical frequency-domain reflectometer by use of Hilbert transformation[J]. *Applied Optics*, 2005, 44(35): 7630-7634.
- [52] Fan X Y, Ito F. Novel optical frequency domain reflectometry with measurement range beyond laser coherence length realized using concatenatively generated reference signal[J]. *Optics InfoBase Conference Papers*, 2007, 32(22): 3227-3229.
- [53] Ding Z Y, Yao X S, Liu T G, et al. Compensation of laser frequency tuning nonlinearity of a long range OFDR using deskew filter[J]. *Optics Express*, 2013, 21(3): 3826-3834.
- [54] Qin J, Zhou Q, Xie W L, et al. Coherence enhancement of a chirped DFB laser for frequency-modulated continuous-wave reflectometry using a composite feedback loop[J]. *Optics Letters*, 2015, 40(19): 4500-4503.
- [55] Feng Y X, Xie W L, Meng Y X, et al. High-performance optical frequency-domain reflectometry based on high-order optical phase-locking-assisted chirp optimization[J]. *Journal of Lightwave Technology*, 2020, 38(22): 6227-6236.
- [56] Zou C, Lin C F, Mou T L, et al. Beyond a 10^7 range-resolution⁻¹ product in an OFDR based on a periodic phase noise estimation method[J]. *Optics Letters*, 2022, 47(20): 5373-5376.
- [57] Galtarossa A, Grosso D, Palmieri L. Accurate characterization of twist-induced optical activity in single-mode fibers by means of polarization-sensitive reflectometry[J]. *IEEE Photonics Technology Letters*, 2009, 21(22): 1713-1715.
- [58] Galtarossa A, Palmieri L. Mapping of intense magnetic fields based on polarization sensitive reflectometry in single mode optical fibers[C]//2013 Africon, September 9-12, 2013, Pointe aux Piments, Mauritius. New York: IEEE Press, 2014.
- [59] Du Y, Jothibasu S, Zhuang Y Y, et al. Rayleigh backscattering based macrobending single mode fiber for distributed refractive index sensing[J]. *Sensors and Actuators B: Chemical*, 2017, 248: 346-350.
- [60] Ding Z Y, Wang C H, Liu K, et al. Distributed measurements of external force induced local birefringence in spun highly birefringent optical fibers using polarimetric OFDR[J]. *Optics Express*, 2019, 27(2): 951-964.
- [61] Froggatt M, Moore J. High-spatial-resolution distributed strain measurement in optical fiber with Rayleigh scatter[J]. *Applied Optics*, 1998, 37(10): 1735-1740.
- [62] Kregar S T, Gifford D K, Froggatt M E, et al. High resolution distributed strain or temperature measurements in single- and multi-mode fiber using swept-wavelength interferometry[C]//Optical Fiber Sensors, October 23-27, 2006, Cancún, Mexico. Washington, DC: OSA, 2006: ThE42.
- [63] Li W H, Chen L, Bao X Y. Compensation of temperature and strain coefficients due to local birefringence using optical

- frequency domain reflectometry[J]. *Optics Communications*, 2013, 311: 26-32.
- [64] Ding Z Y, Wang C H, Liu K, et al. Distributed optical fiber sensors based on optical frequency domain reflectometry: a review[J]. *Sensors*, 2018, 18(4): 1072.
- [65] Zhu T Y, Lin C F, Yang J, et al. Improve accuracy and measurement range of sensing in km-level OFDR using spectral splicing method[J]. *Optics Express*, 2023, 31(13): 20980-20993.
- [66] Yang J, Zou C, Lin C F, et al. Noise compensation methods for optical fiber frequency sweeping interferometry: a review[J]. *Journal of Lightwave Technology*, 2023, 41(13): 4035-4050.
- [67] Gollub J N, Yurduseven O, Trofatter K P, et al. Large metasurface aperture for millimeter wave computational imaging at the human-scale[J]. *Scientific Reports*, 2017, 7: 42650.
- [68] Yurduseven O, Imani M F, Odabasi H, et al. Resolution of the frequency diverse metamaterial aperture imager[J]. *Progress in Electromagnetics Research*, 2015, 150: 97-107.
- [69] Ayhan S, Scherr S, Bhutani A, et al. Impact of frequency ramp nonlinearity, phase noise, and SNR on FMCW radar accuracy [J]. *IEEE Transactions on Microwave Theory and Techniques*, 2016, 64(10): 3290-3301.
- [70] Venkatesh S, Sorin W V. Phase noise considerations in coherent optical FMCW reflectometry[J]. *Journal of Lightwave Technology*, 1993, 11(10): 1694-1700.
- [71] Gorju G, Crozatier V, Lavielle V, et al. Experimental investigation of deterministic and stochastic frequency noises of a rapidly frequency chirped laser[J]. *The European Physical Journal Applied Physics*, 2005, 30(3): 175-183.
- [72] Lin C F, Yang J, Yu Z J, et al. Increased spurious-free dynamic range in frequency sweeping interferometry by suppression of parasitic amplitude modulation[J]. *Journal of Lightwave Technology*, 2022, 40(21): 7191-7199.
- [73] Song J, Li W H, Lu P, et al. Long-range high spatial resolution distributed temperature and strain sensing based on optical frequency-domain reflectometry[J]. *IEEE Photonics Journal*, 2014, 6(3): 6801408.
- [74] Ahn T J, Kim D Y. Analysis of nonlinear frequency sweep in high-speed tunable laser sources using a self-homodyne measurement and Hilbert transformation[J]. *Applied Optics*, 2007, 46(13): 2394-2400.
- [75] Ding Z Y, Liu T G, Meng Z, et al. Note: improving spatial resolution of optical frequency-domain reflectometry against frequency tuning nonlinearity using non-uniform fast Fourier transform[J]. *The Review of Scientific Instruments*, 2012, 83(6): 066110.
- [76] Xing J J, Zhang Y, Wang F, et al. A method based on time-scale factor for correcting the nonlinear frequency sweeping in an OFDR system[J]. *IEEE Photonics Journal*, 2019, 11(3): 7101808.
- [77] Badar M, Lu P, Buric M, et al. Integrated auxiliary interferometer for self-correction of nonlinear tuning in optical frequency domain reflectometry[J]. *Journal of Lightwave Technology*, 2020, 38(21): 6097-6103.
- [78] Guo Z, Han G C, Yan J Z, et al. Ultimate spatial resolution realisation in optical frequency domain reflectometry with equal frequency resampling[J]. *Sensors*, 2021, 21(14): 4632.
- [79] Yu Z J, Zhuang Q Q, Zhu T Y, et al. Distributed polarization crosstalk measurement based on optical frequency domain polarimetry[C]//2021 19th International Conference on Optical Communications and Networks (ICOON), August 23-27, 2021, Qufu, China. New York: IEEE Press, 2021.
- [80] Koshikiya Y, Fan X Y, Ito F. Long range and cm-level spatial resolution measurement using coherent optical frequency domain reflectometry with SSB-SC modulator and narrow linewidth fiber laser[J]. *Journal of Lightwave Technology*, 2008, 26(18): 3287-3294.
- [81] Xie W L, Meng Y X, Feng Y X, et al. Optical linear frequency sweep based on a mode-spacing swept comb and multi-loop phase-locking for FMCW interferometry[J]. *Optics Express*, 2021, 29(2): 604-614.
- [82] Meng Y X, Xie W L, Feng Y X, et al. Dynamic range enhanced optical frequency domain reflectometry using dual-loop composite optical phase-locking[J]. *IEEE Photonics Journal*, 2021, 13(4): 7100307.
- [83] Fan X Y, Koshikiya Y, Ito F. Centimeter-level spatial resolution over 40 km realized by bandwidth-division phase-noise-compensated OFDR[J]. *Optics Express*, 2011, 19(20): 19122-19128.
- [84] Zhang Z P, Fan X Y, Wu M S, et al. Phase-noise-compensated OFDR realized using hardware-adaptive algorithm for real-time processing[J]. *Journal of Lightwave Technology*, 2019, 37(11): 2634-2640.
- [85] Du Y, Liu T G, Ding Z Y, et al. Method for improving spatial resolution and amplitude by optimized deskew filter in long-range OFDR[J]. *IEEE Photonics Journal*, 2014, 6(5): 7902811.
- [86] Zhang Z P, Fan X Y, He Z Y. Long-range distributed static strain sensing with <100 nano-strain resolution realized using OFDR[J]. *Journal of Lightwave Technology*, 2019, 37(18): 4590-4596.
- [87] Chen D, Liu Q W, He Z Y. 108-km distributed acoustic sensor with $220\text{-}\mu\epsilon/\sqrt{\text{Hz}}$ strain resolution and 5-m spatial resolution[J]. *Journal of Lightwave Technology*, 2019, 37(18): 4462-4468.
- [88] Fernández-Ruiz M R, Costa L, Martins H F. Distributed acoustic sensing using chirped-pulse phase-sensitive OTDR technology[J]. *Sensors*, 2019, 19(20): 4368.
- [89] Li H, Liu Q W, Chen D, et al. Centimeter spatial resolution distributed temperature sensor based on polarization-sensitive optical frequency domain reflectometry[J]. *Journal of Lightwave Technology*, 2021, 39(8): 2594-2602.
- [90] 潘浩, 曲兴华, 史春钊, 等. 激光调频连续波测距的精度评定方法研究[J]. *物理学报*, 2018, 67(9): 090201.
- Pan H, Qu X H, Shi C Z, et al. Precision evaluation method of measuring frequency modulated continuous wave laser distance [J]. *Acta Physica Sinica*, 2018, 67(9): 090201.
- [91] Costa L, Martins H F, Martín-López S, et al. Fully distributed optical fiber strain sensor with $10^{-12} \epsilon/\sqrt{\text{Hz}}$ sensitivity[J]. *Journal of Lightwave Technology*, 2019, 37(18): 4487-4495.
- [92] Zhao S Y, Cui J W, Suo L J, et al. Performance investigation of OFDR sensing system with a wide strain measurement range [J]. *Journal of Lightwave Technology*, 2019, 37(15): 3721-3727.
- [93] Lu Y L, Zhu T, Chen L, et al. Distributed vibration sensor based on coherent detection of phase-OTDR[J]. *Journal of Lightwave Technology*, 2010, 28(22): 3243-3249.
- [94] Koyamada Y, Imahama M, Kubota K, et al. Fiber-optic distributed strain and temperature sensing with very high measurand resolution over long range using coherent OTDR[J]. *Journal of Lightwave Technology*, 2009, 27(9): 1142-1146.
- [95] Ding Z Y, Yao X S, Liu T G, et al. Long-range vibration sensor based on correlation analysis of optical frequency-domain reflectometry signals[J]. *Optics Express*, 2012, 20(27): 28319-28329.
- [96] Liu T G, Du Y, Ding Z Y, et al. 40-km OFDR-based distributed disturbance optical fiber sensor[J]. *IEEE Photonics Technology Letters*, 2016, 28(7): 771-774.
- [97] Guo Z, Yan J Z, Han G C, et al. High sensing accuracy realisation with millimetre/sub-millimetre resolution in optical frequency domain reflectometer[J]. *Journal of Lightwave Technology*, 2022, 40(12): 4050-4056.
- [98] Qu S, Wang Z Q, Qin Z G, et al. Internet of things infrastructure based on fast, high spatial resolution, and wide measurement range distributed optic-fiber sensors[J]. *IEEE Internet of Things Journal*, 2022, 9(4): 2882-2889.
- [99] Li P F, Fu C L, Du B, et al. High-spatial-resolution strain

- sensor based on distance compensation and image wavelet denoising method in OFDR[J]. *Journal of Lightwave Technology*, 2021, 39(19): 6334-6339.
- [100] Feng K P, Zu W L, Dang H, et al. Robustness- and processing-rate-improved OFDR based on local search and Kalman prediction[J]. *IEEE Photonics Technology Letters*, 2022, 34(24): 1325-1328.
- [101] Feng K P, Cui J W, Jiang D, et al. Improvement of the strain measurable range of an OFDR based on local similar characteristics of a Rayleigh scattering spectrum[J]. *Optics Letters*, 2018, 43(14): 3293-3296.
- [102] Suo L J, Lei Z K, Takezawa A, et al. Reliability-guided Rayleigh backscattering spectrum correlation method for distributed strain measurements in optical fibres[J]. *Journal of Modern Optics*, 2019, 66(5): 512-520.
- [103] Wang C H, Liu K, Ding Z Y, et al. GPU-based real-time distributed dynamic strain sensing in optical frequency domain reflectometry[J]. *IEEE Sensors Journal*, 2021, 21(21): 24166-24176.
- [104] Taylor H F, Lee C E. Apparatus and method for fiber optic intrusion sensing: US5194847[P]. 1993-03-16.
- [105] 何祖源, 刘庆文. 光纤分布式声波传感器原理与应用[J]. *激光与光电子学进展*, 2021, 58(13): 1306001.
He Z Y, Liu Q W. Principles and applications of optical fiber distributed acoustic sensors[J]. *Laser & Optoelectronics Progress*, 2021, 58(13): 1306001.
- [106] Pedraza A, del Rio D, Bautista-Juzgado V, et al. Study of the feasibility of decoupling temperature and strain from a ϕ -PA-OFDR over an SMF using neural networks[J]. *Sensors*, 2023, 23(12): 5515.
- [107] Wang C H, Liu K, Ding Z Y, et al. High sensitivity distributed static strain sensing based on differential relative phase in optical frequency domain reflectometry[J]. *Journal of Lightwave Technology*, 2020, 38(20): 5825-5836.
- [108] Liu J F, Li C, Fan X J, et al. A method of phase demodulation of OFDR based on ARC-DSM algorithm[J]. *Optoelectronics Letters*, 2022, 18(1): 13-17.
- [109] Feng W, Wang M F, Jia H L, et al. High precision phase-OFDR scheme based on fading noise suppression[J]. *Journal of Lightwave Technology*, 2022, 40(3): 900-908.
- [110] Meng Y J, Fu C L, Chen L, et al. Submillimeter-spatial-resolution ϕ -OFDR strain sensor using femtosecond laser induced permanent scatters[J]. *Optics Letters*, 2022, 47(23): 6289-6292.
- [111] Zhang C, Bao Y, Cui T, et al. Polarization independent phase-OFDR in Rayleigh-based distributed sensing[J]. *Journal of Lightwave Technology*, 2023, 41(8): 2518-2525.
- [112] Wang M F, Feng W, Xie K, et al. Wide measurement range distributed strain sensing with phase-accumulation optical frequency domain reflectometry[J]. *Journal of Lightwave Technology*, 2022, 40(15): 5307-5315.
- [113] 陈典. 基于时间门控数字光频域反射仪的高性能光纤分布式声波传感系统研究[D]. 上海: 上海交通大学, 2022.
Chen D. Research on high performance optical fiber distributed acoustic wave sensing system based on time-gated digital optical frequency domain reflector[D]. Shanghai: Shanghai Jiao Tong University, 2022.
- [114] Cheng Y Y, Luo M M, Liu J F, et al. Numerical analysis and recursive compensation of position deviation for a sub-millimeter resolution OFDR[J]. *Sensors*, 2020, 20(19): 5540.
- [115] Wang Q R, Zhao K H, Badar M, et al. Improving OFDR distributed fiber sensing by fibers with enhanced Rayleigh backscattering and image processing[J]. *IEEE Sensors Journal*, 2022, 22(19): 18471-18478.
- [116] Cui J W, Zhao S Y, Yang D, et al. Investigation of the interpolation method to improve the distributed strain measurement accuracy in optical frequency domain reflectometry systems[J]. *Applied Optics*, 2018, 57(6): 1424-1431.
- [117] Zhao S Y, Cui J W, Wu Z J, et al. Accuracy improvement in OFDR-based distributed sensing system by image processing[J]. *Optics and Lasers in Engineering*, 2020, 124: 105824.
- [118] Qu S, Qin Z G, Xu Y P, et al. High spatial resolution investigation of OFDR based on image denoising methods[J]. *IEEE Sensors Journal*, 2021, 21(17): 18871-18876.
- [119] Pan M, Hua P D, Ding Z Y, et al. Long distance distributed strain sensing in OFDR by BM3D-SAPCA image denoising[J]. *Journal of Lightwave Technology*, 2022, 40(24): 7952-7960.
- [120] Feng K P, Cui J W, Dang H, et al. A OFDR signal processing method based on wavelet transform for improving its sensing performance[J]. *IEEE Photonics Technology Letters*, 2019, 31(13): 1108-1111.
- [121] Gifford D K, Soller B J, Wolfe M S, et al. Optical vector network analyzer for single-scan measurements of loss, group delay, and polarization mode dispersion[J]. *Applied Optics*, 2005, 44(34): 7282-7286.
- [122] Usman A, Zulkifli N, Salim M R, et al. Optical link monitoring in fibre-to-the-x passive optical network (FTTx PON): a comprehensive survey[J]. *Optical Switching and Networking*, 2020, 39: 100596.
- [123] Asha'ari A F A, Bakar A A A, Naim N F. Design of optical frequency domain reflectometer (OFDR) interferometer based on fiber Bragg grating (FBG) for passive optical network (PON) monitoring[C]//2018 IEEE 7th International Conference on Photonics (ICP), April 9-11, 2018, Langkawi, Malaysia. New York: IEEE Press, 2018.
- [124] Ohno S, Iida D, Toge K, et al. Distributed spatial mode dispersion measurement along strongly coupled multicore fiber with C-OFDR[C]//2017 European Conference on Optical Communication (ECOC), September 17-21, 2017, Gothenburg, Sweden. New York: IEEE Press, 2018.
- [125] Podschus J, Koepfel M, Schmauss B, et al. Position measurement of multiple microparticles in hollow-core photonic crystal fiber by coherent optical frequency domain reflectometry [C]//Optical Fiber Sensors Conference 2020 Special Edition, June 8-12, 2020, Washington, DC. Washington, DC: Optica Publishing Group, 2021: W1.2.
- [126] Chen S, Liu Z Y, Niu X C, et al. The scattering characteristic analysis of various types of fiber used in FOCT through OFDR technology[J]. *Proceedings of SPIE*, 2022, 12321: 123210W.
- [127] Zhao D, Pustakhod D, Williams K, et al. Characterization of distributed Bragg reflectors using optical frequency domain reflectometry[C]//2018 IEEE Photonics Conference (IPC), September 30-October 4, 2018, Reston, VA, USA. New York: IEEE Press, 2018.
- [128] Bru L A, Pastor D, Muñoz P. Integrated optical frequency domain reflectometry device for characterization of complex integrated devices[J]. *Optics Express*, 2018, 26(23): 30000-30008.
- [129] Tokushima M, Ushida J. Demonstration of in-depth analysis of silicon photonics circuits using OFDR: waveguides with grating couplers[J]. *Optics Letters*, 2021, 47(1): 162-165.
- [130] Kamata M, Baba T. OFDR analysis of Si photonics FMCW LiDAR chip[J]. *Optics Express*, 2023, 31(15): 25245-25252.
- [131] 付彩玲, 彭振威, 李鹏飞, 等. OFDR 分布式光纤温度/应变/形状传感研究进展[J]. *激光与光电子学进展*, 2023, 60(11): 1106007.
Fu C L, Peng Z W, Li P F, et al. Research on distributed fiber temperature/strain/shape sensing based on OFDR[J]. *Laser & Optoelectronics Progress*, 2023, 60(11): 1106007.
- [132] 马琦琦, 冯忠耀, 王若晖, 等. 面向管线监测的分布式光纤传感土壤传热研究[J]. *光子学报*, 2023, 52(6): 0606002.
Ma Q Q, Feng Z Y, Wang R H, et al. Research on soil heat transfer with distributed optical fiber sensing for pipeline monitoring[J]. *Acta Photonica Sinica*, 2023, 52(6): 0606002.

- [133] 赵艳夺, 王目光, 张静, 等. 高空间分辨率大带宽分布式光纤振动传感系统[J]. 光学学报, 2022, 42(19): 1906004.
Zhao Y D, Wang M G, Zhang J, et al. Distributed optical fiber vibration sensing system with high spatial resolution and large bandwidth[J]. Acta Optica Sinica, 2022, 42(19): 1906004.
- [134] Shao C, Yin G L, Lv L, et al. OFDR with local spectrum matching method for optical fiber shape sensing[J]. Applied Physics Express, 2019, 12(8): 082010.
- [135] Lally E M, Reaves M, Horrell E, et al. Fiber optic shape sensing for monitoring of flexible structures[J]. Proceedings of SPIE, 2012, 8345: 83452Y.
- [136] Matsumoto H, Araki E, Kimura T, et al. Detection of hydroacoustic signals on a fiber-optic submarine cable[J]. Scientific Reports, 2021, 11: 2797.
- [137] Ajo-Franklin J B, Dou S, Lindsey N J, et al. Distributed acoustic sensing using dark fiber for near-surface characterization and broadband seismic event detection[J]. Scientific Reports, 2019, 9: 1328.
- [138] Kishida K, Guzik A, Nishiguchi K, et al. Development of real-time time gated digital (TGD) OFDR method and its performance verification[J]. Sensors, 2021, 21(14): 4865.
- [139] Badar M, Lu P, Wang Q R, et al. Monitoring internal power transformer temperature using distributed optical fiber sensors[J]. Proceedings of SPIE, 2020, 11405: 114050F.
- [140] Zhu L Q, Sun G K, Bao W M, et al. Structural deformation monitoring of flight vehicles based on optical fiber sensing technology: a review and future perspectives[J]. Engineering, 2022, 16: 39-55.
- [141] Coscetta A, Minardo A, Olivares L, et al. Wind turbine blade monitoring with Brillouin-based fiber-optic sensors[J]. Journal of Sensors, 2017, 2017: 9175342.
- [142] 戴建平, 邱锦波, 刘宏睿, 等. 基于内调制DFB激光器的高空间分辨率TGD-OFDR[J]. 光学学报, 2023, 43(7): 0728001.
Dai J P, Qiu J B, Liu H R, et al. High spatial resolution TGD-OFDR based on internally modulated DFB laser[J]. Acta Optica Sinica, 2023, 43(7): 0728001.
- [143] Pillon J, Louf F, Boiron H, et al. Thermomechanical analysis of the effects of homogeneous thermal field induced in the sensing coil of a fiber-optic gyroscope[J]. Finite Elements in Analysis and Design, 2022, 212: 103826.

Advances in High-Performance Optical Frequency Domain Distributed Fiber Optical Measuring and Sensing Technology

Yang Jun^{1,3,4*}, Lin Cuofu², Zou Chen², Yu Zhangjun^{1,3,4}, Wang Yuncai^{1,3,4}, Qin Yuwen^{1,3,4}

¹*Institute of Advanced Photonics Technology, Guangdong University of Technology, Guangzhou 510006, Guangdong, China;*

²*College of Physics and Optoelectronic Engineering, Harbin Engineering University, Harbin 150001, Heilongjiang, China;*

³*Key Laboratory of Photonic Technology for Integrated Sensing and Communication, Ministry of Education of China, Guangzhou 510006, Guangdong, China;*

⁴*Guangdong Provincial Key Laboratory of Information Photonics Technology, Guangzhou 510006, Guangdong, China*

Abstract

Significance Distributed fiber sensing and measurement techniques have been given attractive attention in recent decades due to high sensitivity, high resolution, and large capacity. They have found a wide range of applications in the structural health monitoring of civil infrastructures such as bridges and dams, power-transmission line monitoring, oil-gas extraction and pipeline leakage detection, marine geophysical exploration, dynamic measurement, fiber-optic device characterization, fault diagnosis, etc. On the one hand, distributed measurement techniques can be categorized in principle into scattering effects (including Rayleigh backscattering, Brillouin scattering, and Raman scattering) and coupling effects (polarization crosstalk). On the other hand, these techniques can be divided into optical time domain reflectometry (OTDR), optical frequency domain reflectometry (OFDR), and optical coherence domain reflectometry (OCDR).

OTDR employs the short and high power light pulse for interrogation, which is an effective tool for long distances. However, the tradeoff between sensing length and spatial resolution restricts the measurements to only meter-level spatial resolutions. OCDR utilizes the low coherence light from a broadband light source. They can offer a micrometer-level spatial resolution, whereas the measurement range is less than a few meters. OFDR is a distributed optical fiber measurement method based on the frequency-modulated continuous wave principle in the optical domain. It obtains the characteristics, such as scattering/reflection/loss and polarization features, along the optical fiber according to the mapping relationship between the Fourier transformation frequency of the interference signal and the characteristic location. In addition, the distribution of external physical fields, such as temperature/stress/strain sensing, can be further acquired. Unlike distributed measurement methods based on time-domain or coherent-domain, OFDR offers superior comprehensive properties, including high spatial resolution, high measurement sensitivity, long measurement distance, broad dynamic

range, and high-speed response. However, due to the influence of phase noise, amplitude noise, and environment noise, the performance of OFDR in practice is not satisfactory.

In the past few years, various methods have been proposed to compensate for the laser source noise and environment noise to improve the performance of the OFDR. Distributed sensing based on OFDR is also developing towards high performance and multi-parameters. With the continuous expansion and deepening of the application field, OFDR is facing more daunting challenges, which put forward higher requirements for its measurement performance and anti-interference ability. Therefore, it is of great importance and necessary to provide an overview of recent research progress in existing high-performance OFDR tests and sensing techniques to guide the future development direction.

Progress We first review the measurement principle of OFDR and summarize key technologies to enhance OFDR system performance, such as the noise sources in distributed measurement (Fig. 1), the degradation mechanisms of the spatial point spread function (Fig. 3), and the error or noise compensation techniques. Then, the measurement limit of distributed sensing based on OFDR is derived, and several methods for improving the sensing accuracy and measurement distance are analyzed (Fig. 14). Subsequently, an outline of the current development status of domestic and foreign OFDR instruments is given (Table 6). Besides, application examples are given in measuring integrated waveguide devices, polarization maintaining fibers, and inside stress sensing of optical fiber coil. Finally, several future research directions of OFDR are prospected.

Conclusions and Prospects OFDR systems can provide a good performance of high spatial resolution, high speed, and long measurement and sensing length. This technique can be widely applied to the fields of high-performance fiber optic component measurement and high-precision multi-parameter sensing. In the future, OFDR will continue to develop toward the goal of higher performance, stronger environmental adaptability, and higher measurement cost-effectiveness. The mixed modulation technology such as multi-domain localization (including time, frequency, and coherent domain) and multi-dimensional modulation (including amplitude, phase, and polarization modulation) can provide an effective way to break through the measurement limits and realize the ultra-high performance of OFDR technology. Furthermore, the high-precision OFDR sensing technology should be stepped up to meet the demands of multi-parameter decoupling and anti-interference ability improvement. Correspondingly, for the noise compensation algorithms at present, artificial intelligence and advanced algorithms are all important means for noise suppression capability enhancement and demodulation accuracy improvement. Besides, new requirements are put forward for the small size, low power consumption, and low cost of the core modules in OFDR instruments.

With the continuous innovation of OFDR technology theory and the progress of technology development, China's current overall technology level has achieved international parallelism. However, the typical application fields of OFDR technology need to be continuously expanded, and the advantages of the technology need to be continuously emphasized. In this context, the development of domestic OFDR technology should be highly valued and vigorously developed to realize OFDR technology independent control and localization of hardware, including continuous mode-hopping-free tunable laser source, high-speed and high-precision optoelectronic conversion, and data acquisition module. Moreover, the OFDR technology should gradually move towards engineering applications in the field rather than being confined to laboratory measurements. The environmental adaptability of OFDR instruments should be enhanced to ensure that the core technical indicators of distributed testing and sensing are not degraded in different scenarios. Finally, a high-performance distributed specialized measurement and quantitative sensing methodology should be proposed to promote application development in core fields and typical scenarios, which provides a solid foundation and strong support for satisfying the requirements of applications such as testing of military devices, exploration of oil and gas resources, and power and energy monitoring.

Key words optical frequency domain reflectometry; measuring degradation mechanism; distributed sensing limitation; optical frequency domain reflection instrument; high-performance application